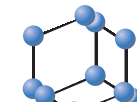
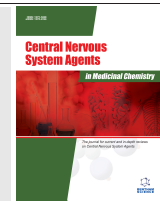


RESEARCH ARTICLE

BENTHAM
SCIENCE

Lead Identification Through *In Silico* Studies: Targeting Acetylcholinesterase Enzyme Against Alzheimer's Disease



Dhairiya Agarwal¹, Sumit Kumar¹, Ramesh Ambatwar¹, Neeru Bhanwala¹, Lokesh Chandrakar¹, and Gopal L. Khatik^{1,*}

¹Department of Medicinal Chemistry, National Institute of Pharmaceutical Education and Research-Raebareli, Uttar Pradesh, 226002, India

Abstract: **Aims:** In this work, we aimed to acquire the best potential small molecule for Alzheimer's disease (AD) treatment using different models in Biovia Discovery Studio to identify new potential inhibitors of acetylcholinesterase (AChE) via *in silico* studies.

Background: The prevalence of cognitive impairment-related neurodegenerative disorders, such as AD, has been observed to escalate rapidly. However, we still know little about the underlying functions, outcome predictors, or intervention targets causing AD.

Objectives: The objective of the study was to optimize and identify the lead compound to target AChE against Alzheimer's disease.

Methods: Different *in silico* studies were employed, including the pharmacophore model, virtual screening, molecular docking, *de novo* evolution model, and molecular dynamics.

Results: The pharmacophoric features of AChE inhibitors were determined by ligand-based pharmacophore models and 3D QSAR pharmacophore generation. Further validation of the best pharmacophore model was done using the cost analysis method, Fischer's randomization method, and test set. The molecules that harmonized the best pharmacophore model with the estimated activity < 1 nM and ADMET parameters were filtered, and 12 molecules were subjected to molecular docking studies to obtain binding energy. 3vsp_EK8_1 secured the highest binding energy of 65.60 kcal/mol. Further optimization led to a 3v_Evo_4 molecule with a better binding energy of 70.17 kcal/mol. The molecule 3v_evo_4 was subjected to 100 ns molecular simulation compared to donepezil, which showed better stability at the binding site.

Conclusion: A lead compound, 3v_Evo_4 molecule, was identified to inhibit AChE, and it could be further studied to develop as a drug with better efficacy than the existing available drugs for treating AD.

Keywords: Alzheimer's disease, molecular docking, pharmacophore models, *de novo* evolution, molecular simulation, *in silico*.

1. INTRODUCTION

Alzheimer's disease (AD) is a progressive, irreversible neuronal brain damage, a common cause of dementia in old-age people. This neuronal disease is a very complicated phenomenon, and the etiology and pathogenesis of AD are still unclear. Due to multi-facet pathways, a single drug is ineffective for treating Alzheimer's disease [1]. The complexity

of AD has been justified by various theories involving the tau protein, oxidative stress (OS), the amyloid cascade, and the cholinergic system (Fig. 1) [2–5]. The reduction in the level of acetylcholine (ACh), an important neurotransmitter involved in memory, attention, and motivation, leads to neuronal damage due to a high level of AChE enzyme responsible for ACh's breakdown [6–8]. According to a recent report from the WHO, the number of people with AD will rise from 50 to 150 million by 2050, placing a significant financial, social, and healthcare burden on the patients and their families [9].

*Address correspondence to this author at the Department of Medicinal Chemistry, National Institute of Pharmaceutical Education and Research-Raebareli, Uttar Pradesh, 226002, India; Tel: +919256336645; E-mail: gopal_niper@rediffmail.com

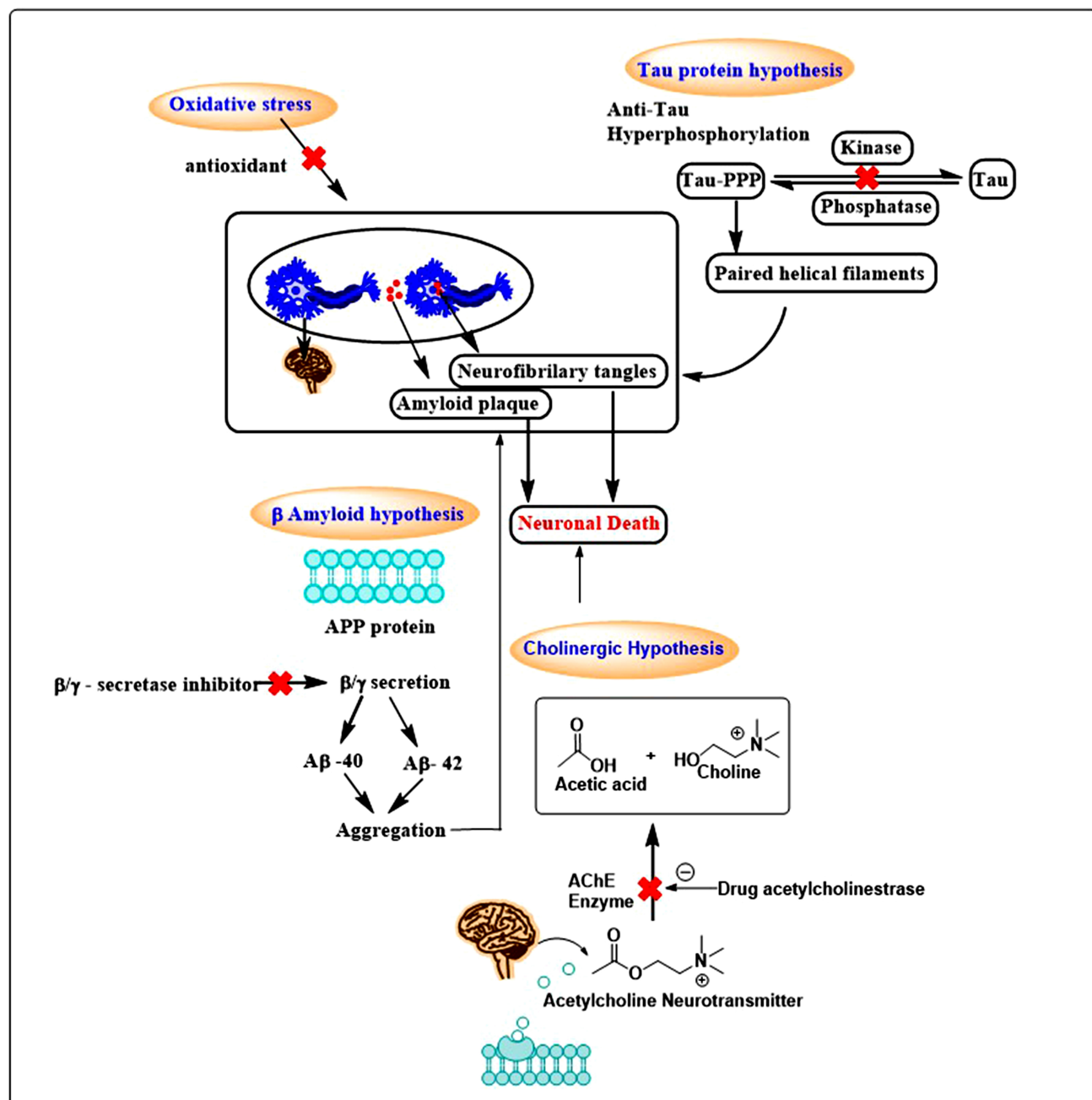


Fig. (1). Pathomechanism of alzheimer's disease. (*A higher resolution / colour version of this figure is available in the electronic copy of the article*).

In the case of the “amyloid hypothesis”, the production and accumulation of oligomeric aggregates of amyloid- β (A β_{42}) peptide in the brain are central events in the pathogenesis of AD [10, 11]. The hippocampus, entorhinal cortex, and prefrontal cortex are three key brain regions that play crucial roles in the cognitive and memory deficits observed in AD. The hippocampus, specifically its CA1 and subiculum regions, is susceptible to the buildup of amyloid-beta and tau proteins. This accumulation contributes to synaptic dysfunction and the loss of neurons. Consequently, impairment of the hippocampus significantly hampers memory, particularly the ability to create new memories, which is a

characteristic feature of AD; the entorhinal cortex is among the first brain regions to display pathological alterations, marked by the presence of amyloid-beta plaques [12]. This damage to the entorhinal cortex hinders the smooth transmission of information to the hippocampus, leading to difficulties in forming new memories and spatial orientation. The disruption in the prefrontal cortex can lead to difficulties with problem-solving, decision-making, and impaired judgment [13]. It can also contribute to changes in personality and behavior often seen in AD patients; therefore, there is a need for the development of drugs targeting the cholinergic hypothesis. AChE and BuChE inhibitors have been docu-

mented as critical targets for effective AD management by increasing ACh availability in the brain regions [11, 14, 15]. AChE is a ubiquitous serine hydrolase enzyme that ceases nerve impulses by hydrolyzing the neurotransmitter acetylcholine (ACh) to choline and acetate. Its numerous crystal structures are available, which reveals that AChE can control the concentration of ACh at the synapse [16, 17].

ACh plays a significant role in learning ability, memory, and cognitive processes. Both catalytic and peripheral sites are available in the AChE enzyme, to which inhibitors can bind and inhibit its activity [18]. In the forebrain, AChE inhibitors increase cholinergic neurotransmission by reducing the dissociation of acetylcholine. Two major types of cholinesterases (ChEs) in the mammal brain are AChE and BuChE processes [19, 20]. The enzyme BuChE, like AChE, is also involved in the hydrolysis of the neurotransmitter ACh. In AD, which affects the brain, the BuChE level and activity gradually increase, while the activity of AChE decreases. AChE and BuChE combine to regulate the central Ach levels, making them a plausible target [21, 22]. Several AChE inhibitors are used as drugs, like donepezil, rivastigmine, and galantamine, and many more are under investigation [23]. Looking at the potential of computer-aided drug design (CADD), we have explored the various computational techniques to find a potential small molecule for AD treatment. Biovia Discovery Studio 2022 [24] was used to identify new potential AChE inhibitors, employing various *in silico* studies, including pharmacophore modelling, molecular docking, virtual screening, *de novo* evolution, and molecular dynamics. The pharmacophoric features of AChE inhibitors were determined by ligand-based pharmacophore mode and 3D QSAR pharmacophore generation. The best pharmacophore model was validated by the cost analysis method, Fischer's randomization method, and test set, which subsequently led to a potent small molecule to treat AD.

2. MATERIALS AND METHODS

2.1. Generation of the Dataset and Feature Mapping

A set of 40 different AChE inhibitors with the best inhibitory activity, *i.e.*, IC₅₀ in the nM range, were selected from various published sources. The AChE inhibitors dataset was divided into a training set (32 molecules) and a test set (8 molecules). The training set was generated from activity (IC₅₀) ranging from 0.07 nM to 1000 nM (Table 1) to generate the pharmacophore model. The test set was generated based on the inhibitory activity IC₅₀ value ranging from 0.52 nM to 770 nM (Table 2) to assess the produced pharmacophore models [25]. Based on the lower IC₅₀ values, the top two molecules were selected to determine the pharmacophoric features with the feature mapping protocol. The hydrogen bond acceptor (HBA), hydrogen bond donor (HBD), hydrophobic (HY), ring aromatic (RA), and positive ionization (PI) properties were used as key inputs to generate the 3D quantitative structure-activity relationship (3D-QSAR). The biological activity of the inhibitors was either three times higher or three times lower than the genuine value in this case since the uncertainty value of the training set and test set was set to 3. The 3D-QSAR pharmacophore models were

created using the HypoGen module, which received all 32 compounds from the training set (Tables 3–5, Figs. 3, 5, 6) [26]. The best algorithm method was considered as existing conformers led to interrupted search when possible adaptable conformation was set with a 15 kcal/mol of energy limit and the highest conformations were set to be 255 in numbers. Ten pharmacophore models were produced with important statistical parameters, like total cost, root mean square deviation (RMSD), cost difference (Δ Cost), correlation (r^2), and pharmacophore features.

A high correlation coefficient and low RMSD values are assumed ideal for the best pharmacophore model. Thus, model validation was done using various parameters, like the cost analysis method (equation i), Fischer's randomization, and the test set.

$$\Delta\text{Cost} = (\text{null cost} - \text{total cost}) \dots \text{equation (i)}$$

An effective pharmacophore model should have a total cost that is more similar to the fixed cost than the null cost. Theoretically, the quality of the pharmacophore model improves as the Δ cost increases.

Further randomizing the activity levels of the molecules in the training set, Fischer's randomization generated a variety of random spreadsheets based on the significance level (95%) chosen. In our situation, 19 random spreadsheets were produced during the creation of the initial hypothesis. The suitability of the prepared pharmacophore model was evaluated using a test set of 8 chemical compounds with diverse structural characteristics [25, 27].

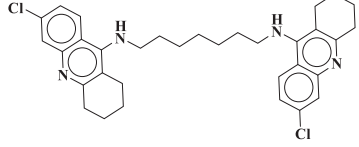
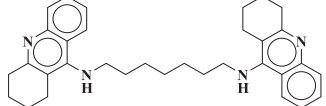
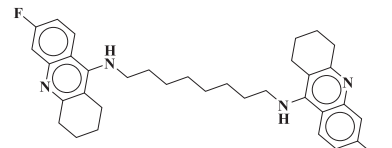
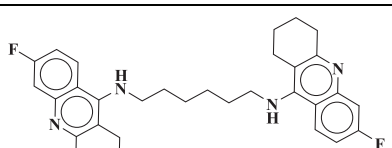
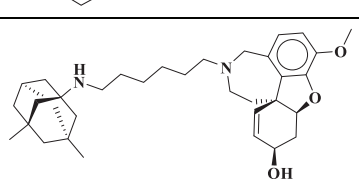
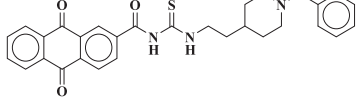
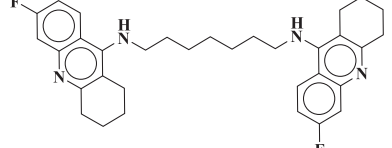
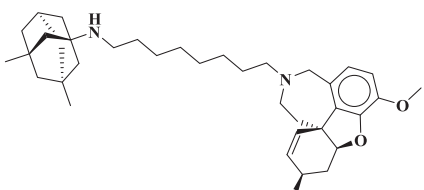
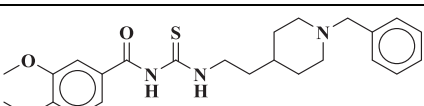
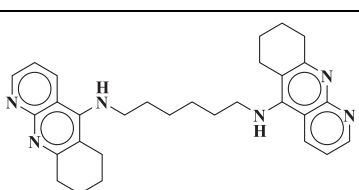
2.2. Virtual Screening and ADMET Studies

To identify potent molecules from five databases (Enamine CNS database, Druglike database, scPDB database, Sample, and MiniMaybridge) that collectively contain over 200,000 chemicals, a highly validated pharmacophore (Hypo1) was employed as a 3D query. The top-performing Hypo1 was utilized to match the chemical properties of the identified hit compounds using the most effective search technique. Furthermore, we selected molecules with a predicted HypoGen activity of less than 1nM, which are considered active compounds. These screened molecules underwent further filtering based on ADMET properties [28]. The ADMET protocol was used to assess properties, such as aqueous solubility, blood-brain barrier penetration (BBB), CYP P4502D6 inhibition, hepatotoxicity, human intestinal absorption (HIA), and plasma protein binding (PPB). Table 6 presents the 19 molecules that exhibited a favorable screened parameter.

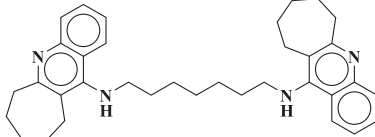
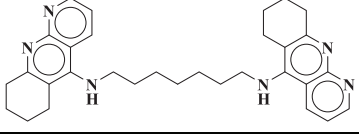
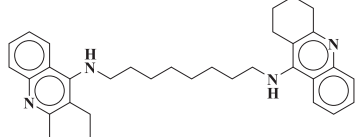
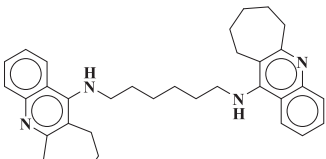
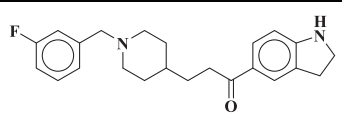
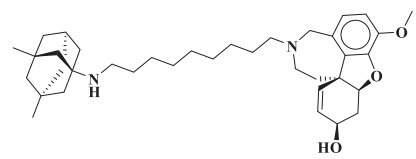
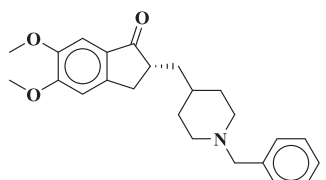
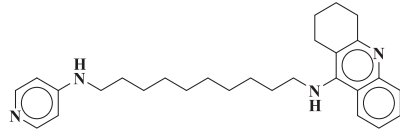
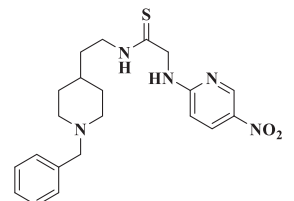
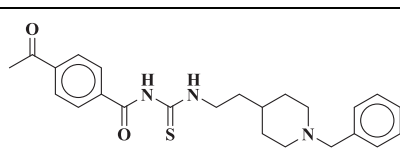
2.3. Molecular Docking, *De Novo* Evolution, and Simulation

The CDOCKER algorithm, based on the CHARMM force field, is used for molecular docking studies [25]. The 3D crystal structure of human AChE was recovered with good resolution (2.45Å) from a protein databank (PDB Id-7E3H) [29]. The choline-binding pocket (Trp86), the acyl-binding pocket (Trp286, Phe295, and Val294), as well as the catalytic residues, serine and histidine (Ser293 and His447),

Table 1. A training set with the experimental activity (IC_{50}) in the nanomolar range.

Entry	Code	Structure	IC_{50} (nM)
1	ChE 1		0.07
2	ChE 2		0.2
3	ChE 3		0.7
4	ChE 4		0.9
5	ChE 5		1.16
6	ChE 6		2
7	ChE 7		0.6
8	ChE 8		5.36
9	ChE 9		5
10	ChE 10		4.8

(Table 1) Contd...

Entry	Code	Structure	IC ₅₀ (nM)
11	ChE 11		2.7
12	ChE 12		1.3
13	ChE 13		1.6
14	ChE 14		2.5
15	ChE 15		16
16	ChE 16		2.32
17	ChE 17		1.7
18	ChE 18		176
19	ChE 19		2.6
20	ChE 20		7.5

(Table 1) Contd...

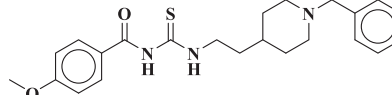
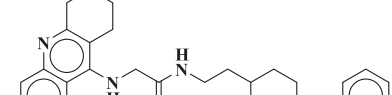
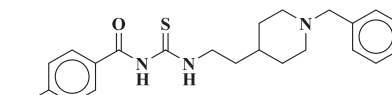
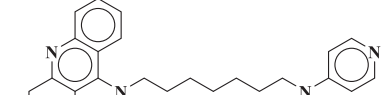
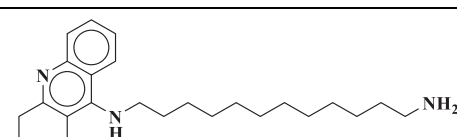
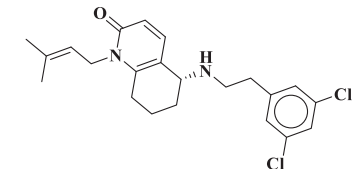
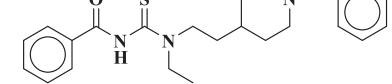
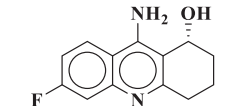
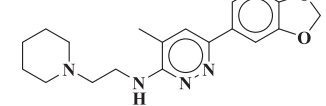
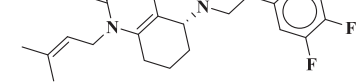
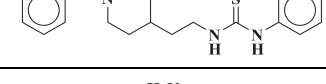
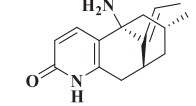
Entry	Code	Structure	IC ₅₀ (nM)
21	ChE 21		10
22	ChE 22		6
23	ChE 23		20
24	ChE 24		302
25	ChE 25		180
26	ChE 26		800
27	ChE 27		300
28	ChE 28		292
29	ChE 29		1,000
30	ChE 30		980
31	ChE 31		850
32	ChE 32		900

Table 2. A test set with the experimental activity (IC_{50}) in the nanomolar range.

Entry	Code	Structure	IC_{50} (nM)
1	ChE 33		1.03
2	ChE 34		0.52
3	ChE 35		4.31
4	ChE 36		1.9
5	ChE 37		7.7
6	ChE 38		770
7	ChE 39		210
8	ChE 40		823

were chosen as the enzyme's active binding site, according to the literature [29]. The Define and Edit binding protocol defined the amino acid residues at the protein active site with 9.35 Å of a radius as the site sphere domain [30]. The top ten conformations were generated for each ligand from the virtual screening procedure after they were docked in the active site of AChE to discover the most appropriate orientation. The candidate molecules were then subjected to *de novo* evolution once the docking findings had been analyzed based on the docking scores [31]. In the protocol of *de novo* evolution, the fragments that were determined to constitute the receptor's ideal complement were evaluated using the LUDI

algorithm. Then, the already-existing molecular skeleton was modified by joining these fragments to the molecules [32, 33]. The type of fragment selection and the creation of novel ligands depend on the mode of evolution. Small pieces from a library were initially added to a scaffold in a protein-active site. Then, using a predetermined collaboration guide, pieces were placed in correlation with the receptor to produce a variety of high-scoring molecules. In this convention, we used full development to choose portions based on the LUDI score, and the boundary value of the largest RMSD for fitting was 1 [34, 35]. The new molecules with high LUDI scores from the *de novo* evolution were docked one more

time to the AChE active site to assess binding poses and binding energies. The molecular docking tool was used to predict the poses for the ligand complexes of AChE-donepezil, and the screened molecules with the best binding conformations were subjected to a 100 ns MD simulation. Using Biovia Discovery Studio 2022, all MD simulations were carried out using pdb Id-7E3H, and the protein-ligand complex was produced. The simulation system for characterizing the motions of the protein atoms was constructed using the CHARMM force field [28]. Each protein-ligand system was solvated in a cubic simulation box of 17328 water, and charges were then balanced by adding 49 Na⁺ and 46 Cl⁻ ions. For the first energy minimization, a steepest descent algorithm was used for 1000 steps, and for the second energy minimization, a conjugate gradient algorithm was used for 1000 steps. The LINCS algorithm was applied to limit bonds to the appropriate length with hydrogen [30]. Production simulations were run for 100 ns under NPT circumstances, while the Newtonian equations of motion were integrated. Lennard-Jones interactions and the particle-mesh Ewald method were used to calculate the interactions within a 2 Å cut-off [36].

3. RESULTS AND DISCUSSION

3.1. Generation of Training and Test Set

A set of 40 chemically diverse inhibitors with a different experimental IC₅₀ value was taken to generate training and test sets [37]. An 80% random approach was split to generate two sets, *i.e.*, 32 molecules comprising a training set (Table 1) and 8 molecules comprising a test set (Table 2). Both sets contained diverse molecules with different activities [38]. A generated training set was used for the 3D-QSAR pharmacophore generation. A test set was used to validate the best hypothesis formed and prove the generated pharmacophores' authenticity.

3.2. Pharmacophore Modeling

The HypoGen method was used to create ten quantitative hypotheses that connected the experimental and estimated activity values using a collection of 32 AChE inhibitors with different chemical compositions. Table 3 lists each hypothesis' relevant statistical parameter values, including cost analysis, correlation coefficient (r^2), and root-mean-square deviation (RMSD). The best hypotheses have a substantial total cost value, the lowest RMSD, the biggest cost difference, and a decent correlation coefficient (close to 1). Therefore, it was determined that the best pharmacophore Hypo1, presented in Table 3, had the greatest overall cost value (148.85), the best correlation coefficient (0.89), the biggest cost difference (58.37), the lowest RMSD (1.12), and the lowest RMSD [39]. Modeling the best HypoGen pharmacophore (Fig. 2A) depicted the chemical characteristics of Hypo1, which included three hydrophobic features (HY), two ring aromatics (RA), and two hydrogen bond acceptors (HBA). The most active compound, with an IC₅₀ value of 0.07 nM, mapped every pharmacophore feature, whereas the most inactive molecule, with an IC₅₀ value of 1000 nM, mapped just three features, as shown in Figs. (2B and C). Hypo1 aligned to both molecules individually. We conclude

from the analysis that Hypo1 was the most effective pharmacophore model, which has also been verified using other techniques, such as Fischer's randomization, cost analysis, and test set. Our assessment, based on the graphical representation of cost difference, fit value, RMSD, and correlation coefficient, firmly established Hypo1 as the most effective pharmacophore model.

3.3. Pharmacophore Model Validation

3.3.1. Cost Analysis

Null and total costs are separated by a cost differential between 40 and 60 bits. Therefore, the projected correlation probability is predicted to be between 75 and 90%. More than 90% of the anticipated correlation probability is deemed to exist if the difference exceeds 60 bits. The fixed cost is a straightforward model that completely matches all the data. The experimental activities are normally distributed around their average value, and the null cost assumes no association between the data. As a result, the validity of Hypo1 also depends on how far away from the null cost and how near to the fixed cost the overall cost value is. The fixed, total, and null cost ratings in this study were 128.721, 148.85, and 207.22, respectively, as revealed by Hypo1. Therefore, hypo1 could be the best hypothesis because of the highest cost difference of around 60 bits, meaning a more than 90% correlation probability.

3.3.2. Validation by Fischer Randomization

The importance of Hypo1 was further validated using the Fischer randomization test based on statistical relevance. To confirm the statistical robustness of Hypo1, 19 random spreadsheets were made with a 95% confidence level. Fig. (4) shows that none of the 19 randomly generated pharmacophore hypotheses had better statistical characteristics than Hypo1, showing that the overall cost value of the 19 hypotheses was greater than Hypo1. The findings confirm the validity of Hypo1 and validate its dependability.

3.3.3. Validation of Training and Test Set

Based on these well-known AChE inhibitors, the 3D-QSAR approach was applied using 32 molecule training sets (Table 1) and 8 molecule test sets (Table 2) to determine if the pharmacophore model could predict the activity in the same activity range. Based on their activity levels, all the training set molecules and the test set were divided into three activity scales: highly active, IC₅₀ < 1 nM; moderately active, 1 nM ≤ IC₅₀ < 100 nM; and less active, IC₅₀ ≥ 100 nM (Tables 4 and 5). Four molecules from the training set (Table 4) were considered inactive or moderately active, while Hypo1 projected others to be in high activity range. These molecules were ChE 18, ChE 24, ChE 25, and ChE 26.

Fig. (7) (Tables S1-S3) displays the greatest correlation coefficient (r^2) of 0.89 between experimental and calculated AChE inhibitory activity levels for the training set. According to the test set presented in Table 5 (Tables S1-S3), the moderately active molecule ChE 35 and the inert molecule ChE 38 were both overestimated as active molecules.

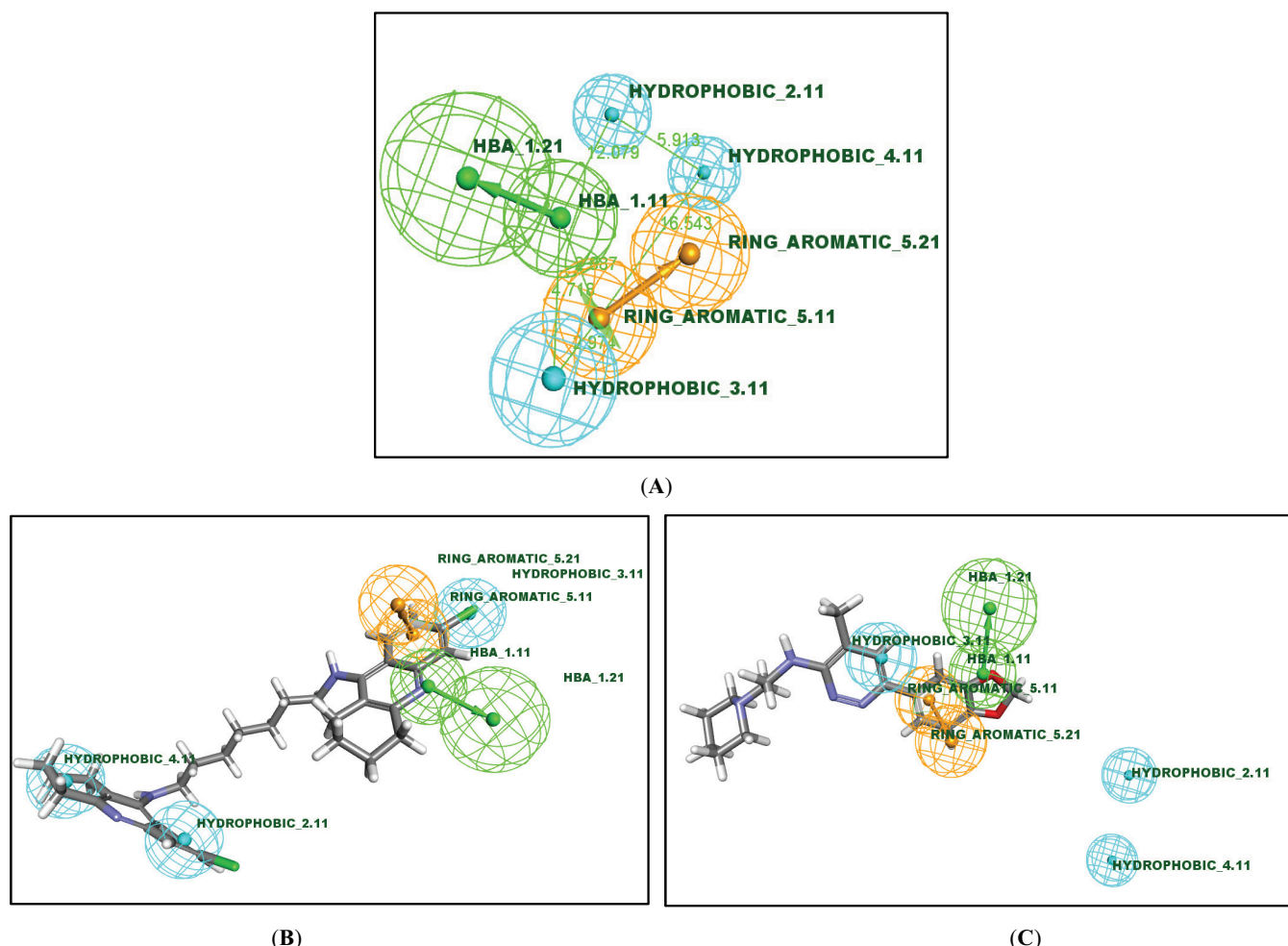


Fig. (2). (A). Best Hypo1 Gen pharmacophore model Hypo1 along with its chemical features. (B) Most active molecule aligned to the Hypo1 ($IC_{50} = 0.07 \text{ nM}$). (C) Most inactive molecule aligned to the Hypo1 ($IC_{50} = 1000 \text{ nM}$). (A higher resolution / colour version of this figure is available in the electronic copy of the article).

Table 3. The HypoGen algorithm for AChE inhibitors with 10 pharmacophore models.

Hypo	Total Cost	Cost Difference ^a	Maximum Fit	RMSD ^b	Correlation (r^2)	Properties
1	148.85	58.37	10.61	1.12	0.89	HBA, 3HY, RA
2	155.40	51.82	9.23	1.28	0.86	HBA, 2HY, RA
3	158.33	48.89	9.41	1.36	0.84	HBA, 3HY, RA
4	158.41	48.81	7.22	1.36	0.84	HBA, 2HY, RA
5	158.42	48.80	7.12	1.36	0.84	HBA, 2HY, RA
6	159.00	48.23	9.03	1.37	0.84	2HBA, HY, RA
7	159.32	47.90	8.01	1.38	0.83	HBA, HBD, HY, RA
8	159.66	47.56	9.08	1.38	0.83	HBA, 2HY, RA
9	159.91	47.32	8.54	1.39	0.83	2HBA, HY, RA
10	160.48	46.74	6.39	1.39	0.83	HBA, HY, 2RA

Note: ^aCost difference: (null cost - total cost); null cost = 207.22, fixed cost = 128.721. Abbreviations: Hydrogen bond acceptors (HBA), hydrogen bond donors (HBD), hydrophobic (HY), and ring aromatic (RA). ^bRMSD: the variation of the log (estimated activities) from the log (measured activities).

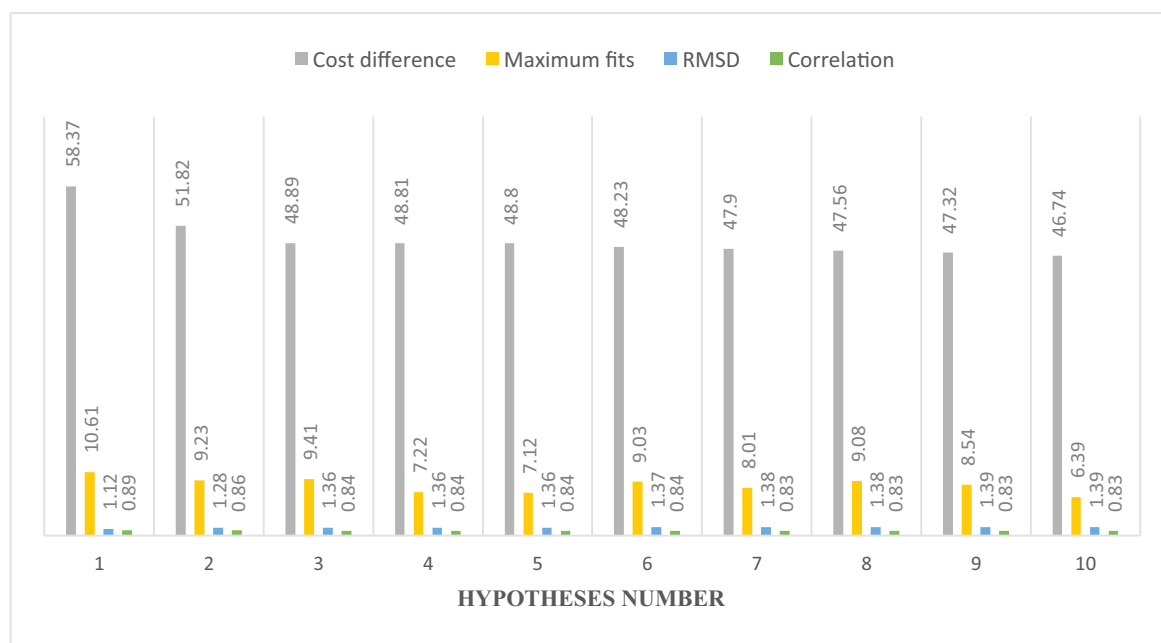


Fig. (3). Graphical representation of 10 hypotheses for AChE inhibitors (HypoGen algorithm). (*A higher resolution / colour version of this figure is available in the electronic copy of the article*).

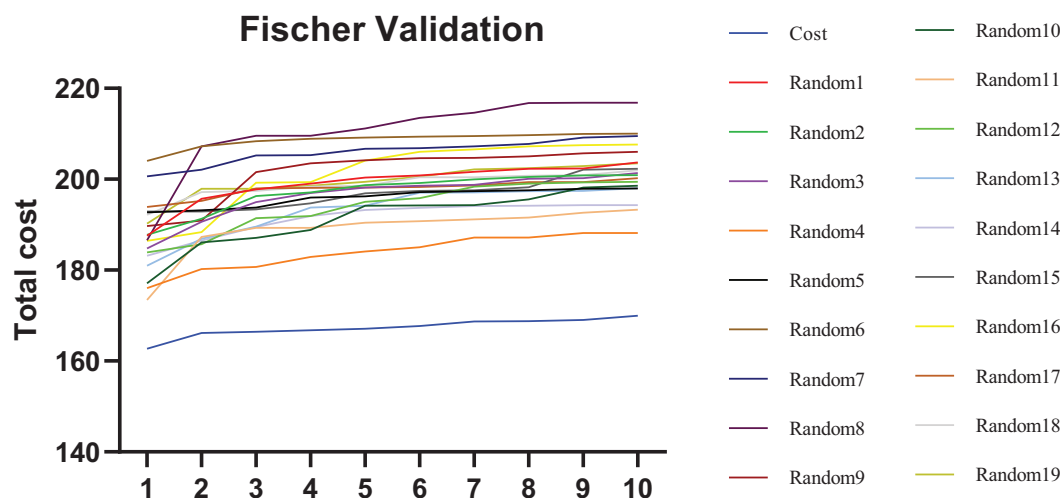


Fig. (4). Fischer validation (total cost of the initial and the 19 random spreadsheets at 95% confidence level). (*A higher resolution / colour version of this figure is available in the electronic copy of the article*).

All the molecules in the test set, apart from these two, have been predicted by Hypo1 to be within their respective activity ranges. The correlation coefficient (r^2) between experimental and estimated AChE inhibitory activity levels for the test set was 0.68. These findings suggested that Hypo1 was appropriate for the training set and could accurately measure the inhibitory activity (Fig. 8, Table S2). Thus, the Hypo1 model can be used to identify the probable AChE inhibitors.

3.3.4. Virtual Screening

We screened 1088 compounds for further examination after collecting unique candidate molecules from five databases. 222 molecules were identified as active since they had

estimated activity values of less than 1 nM [40]. These 222 molecules were prepared and reduced using the steps of minimise ligands and prepare or filter ligands. These two steps resulted in the production of 106 molecules, which were then assessed *in silico* for their physicochemical (ADMET) characteristics, such as aqueous solubility, blood-brain barrier penetration (BBB), cytochrome P4502D6 inhibition, hepatotoxicity, human intestinal absorption (HIA), and plasma protein binding (PPB) (Fig. 9 and Table 6). According to the findings, 19 hits had good ADMET qualities compared to reference ADMET attributes (Table S3) [41]. The virtual screening procedure produced these hit compounds, which were later screened.

Table 4. Hypo1-generated estimated activity of the training set molecules.

Entry	Molecule	^a Fit Value	Estimated Activity (IC ₅₀ = nM)	Activity (IC ₅₀ = nM)	^b Error	^c Activity Scale
1	ChE 1	9	0.06	0.07	-1.12	Active
2	ChE 2	8.06	0.54	0.2	2.72	Active
3	ChE 3	7.92	0.76	0.7	1.09	Active
4	ChE 4	7.85	0.89	0.9	-1.01	Active
5	ChE 5	7.83	0.94	1.16	-1.24	Moderately active
6	ChE 6	7.79	1.03	2	-1.95	Moderately active
7	ChE 7	7.78	1.05	0.6	1.75	Moderately active
8	ChE 8	7.52	1.89	5.36	-2.83	Moderately active
9	ChE 9	7.5	1.97	5	-2.54	Moderately active
10	ChE 10	7.49	2.03	4.8	-2.36	Moderately active
11	ChE 11	7.48	2.08	2.7	-1.30	Moderately active
12	ChE 12	7.4	2.53	1.3	1.94	Moderately active
13	ChE 13	7.34	2.89	1.6	1.81	Moderately active
14	ChE 14	7.11	4.86	2.5	1.94	Moderately active
15	ChE 15	7.09	5.12	16	-3.13	Moderately active
16	ChE 16	7.04	5.8	2.32	2.50	Moderately active
17	ChE 17	6.9	7.9	1.7	4.65	Moderately active
18	ChE 18	6.24	36.11	176	-4.87	Moderately active
19	ChE 19	6.21	38.82	2.6	14.93	Moderately active
20	ChE 20	6.17	42.31	7.5	5.64	Moderately active
21	ChE 21	6.14	46.07	10	4.61	Moderately active
22	ChE 22	6.1	50.07	6	8.34	Moderately active
23	ChE 23	6.08	51.92	20	2.60	Moderately active
24	ChE 24	6.06	54.35	302	-5.56	Moderately active
25	ChE 25	6.01	62.16	180	-2.90	Inactive
26	ChE 26	5.97	68.05	800	-11.76	Inactive
27	ChE 27	5.79	101.2	300	-2.96	Inactive
28	ChE 28	5.54	182.17	292	-1.60	Inactive
29	ChE 29	5.44	230.22	1,000	-4.34	Inactive
30	ChE 30	5.31	310.2	980	-3.16	Inactive
31	ChE 31	4.85	884.26	850	1.04	Inactive
32	ChE 32	4.24	3593.62	900	3.99	Inactive

Note: ^aFit value measures how closely the chemical characteristics of the molecules in the training set and the features coincide. If the ^berror is positive, the estimated IC₅₀ is more than the experimental IC₅₀, while a negative value suggests the estimated IC₅₀ is less than the experimental IC₅₀ in nM. ^cActivity scale: IC₅₀ < 1 nM = active; 1 nM ≤ IC₅₀ < 100 nM = moderately active; IC₅₀ ≥ 100 nM = inactive.

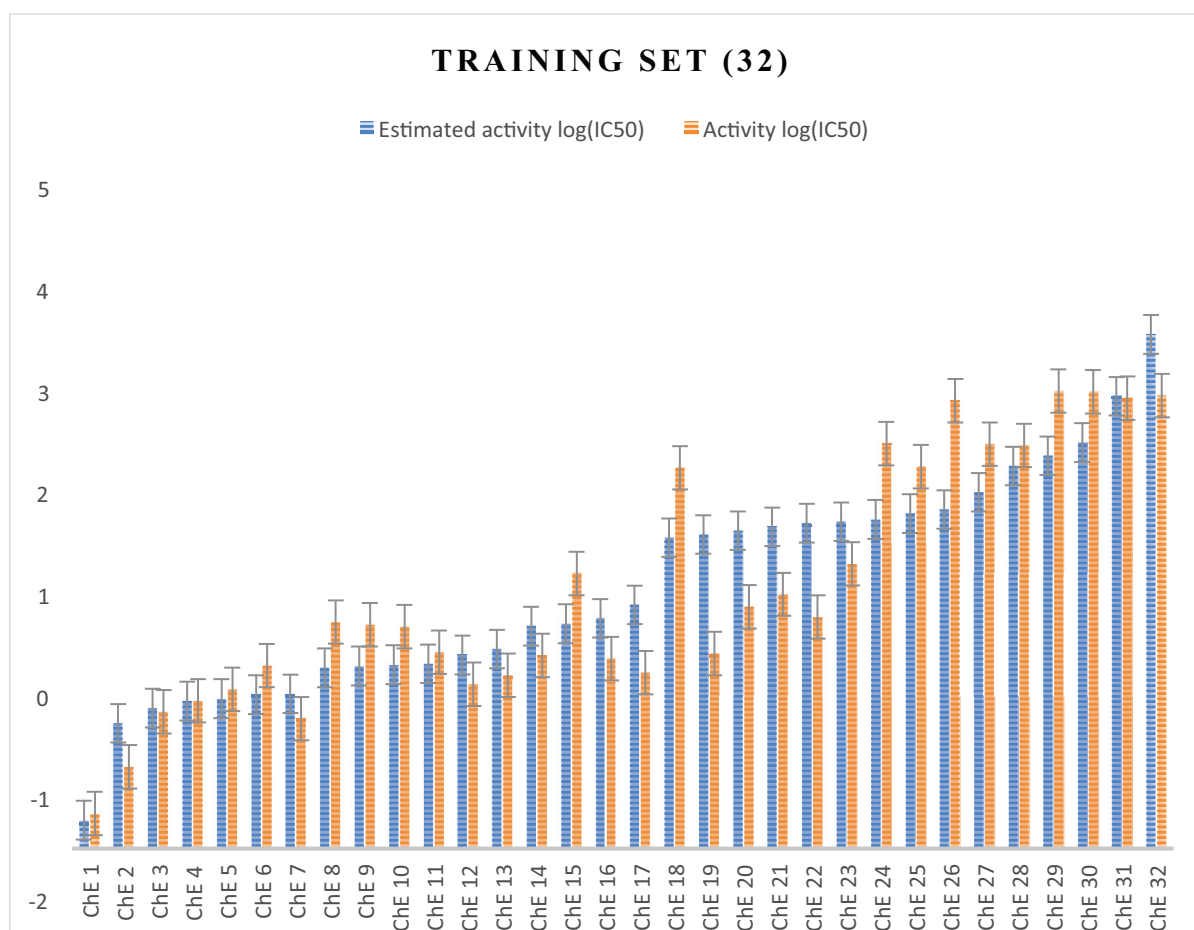


Fig. (5). A graphical representation depicting the relationship between estimated activity log(IC₅₀) values and activity log(IC₅₀) values generated for the training set. (A higher resolution / colour version of this figure is available in the electronic copy of the article).

Table 5. Hypo1-generated predicted activity of the test set molecules.

Entry	Molecule	^a Fit Value	Estimated Activity (IC ₅₀ = nM)	Activity (IC ₅₀ = nM)	^b Error	^c Activity Scale
1	ChE 33	9.13	0.05	1.03	-22.12	Active
2	ChE 34	8.26	0.35	0.52	-1.49	Active
3	ChE 35	8.18	0.41	4.31	-10.41	Active
4	ChE 36	7.58	1.64	1.9	-1.16	Moderately active
5	ChE 37	6.23	37.44	7.7	4.86	Moderately active
6	ChE 38	5.77	105.77	770	-7.28	Moderately active
7	ChE 39	3.43	23565.1	210	112.22	Inactive
8	ChE 40	2.33	2470	823	3	Inactive

Note: ^aFit value measures how closely the chemical characteristics of the molecules in the training set and the features coincide. If the ^berror is positive, the estimated IC₅₀ is more than the experimental IC₅₀, while a negative value suggests the estimated IC₅₀ is less than the experimental IC₅₀ in nM. ^cActivity scale: IC₅₀ < 1 nM = active; 1 nM ≤ IC₅₀ < 100 nM = moderately active; IC₅₀ ≥ 100 nM = inactive.

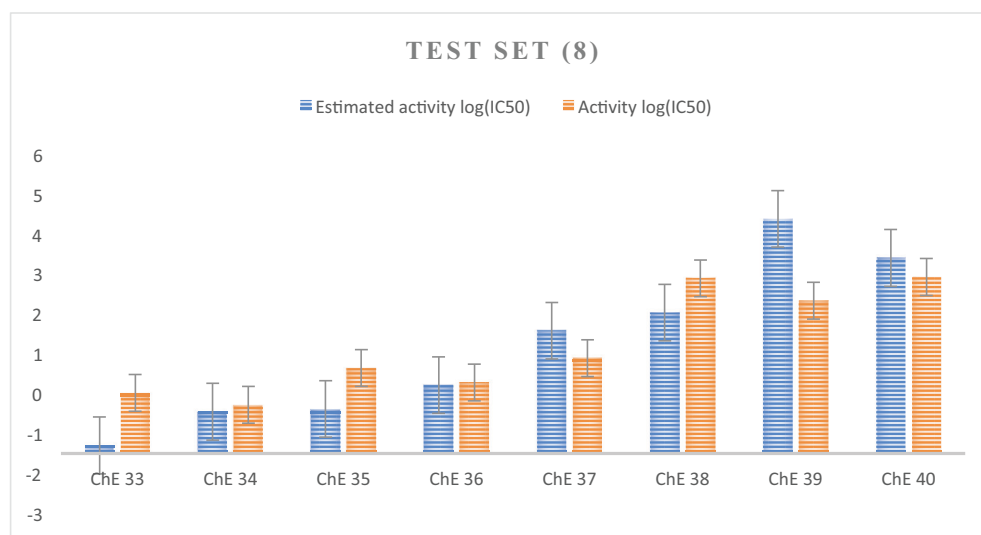


Fig. (6). A graphical representation depicting the relationship between estimated activity $\log(\text{IC}_{50})$ values and activity $\log(\text{IC}_{50})$ values generated for the test set. (A higher resolution / colour version of this figure is available in the electronic copy of the article).

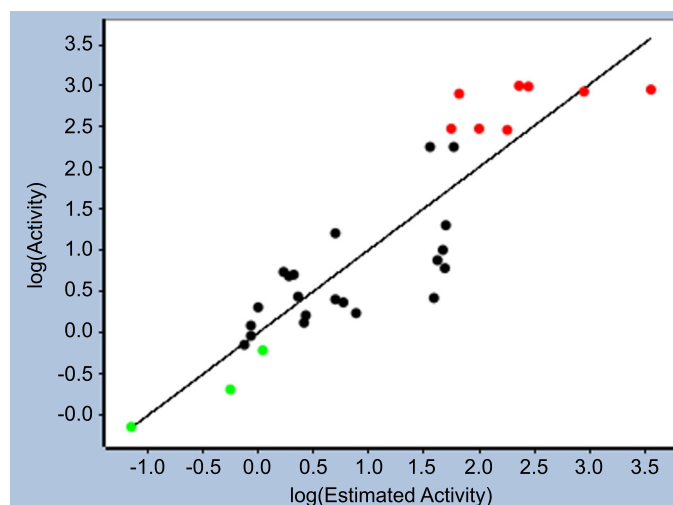


Fig. (7). Correlation of training set's estimated and experimental activity ($\log\text{IC}_{50}$) determined by Hypo1. *Green, black, and red colors represent the nature of molecules. (A higher resolution / colour version of this figure is available in the electronic copy of the article).

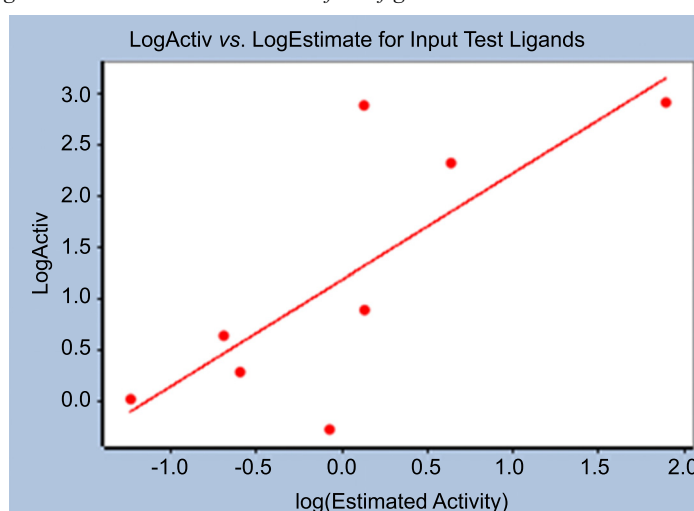


Fig. (8). Correlation of test set's estimated and experimental activity ($\log\text{IC}_{50}$) determined by Hypo1. (A higher resolution / colour version of this figure is available in the electronic copy of the article).

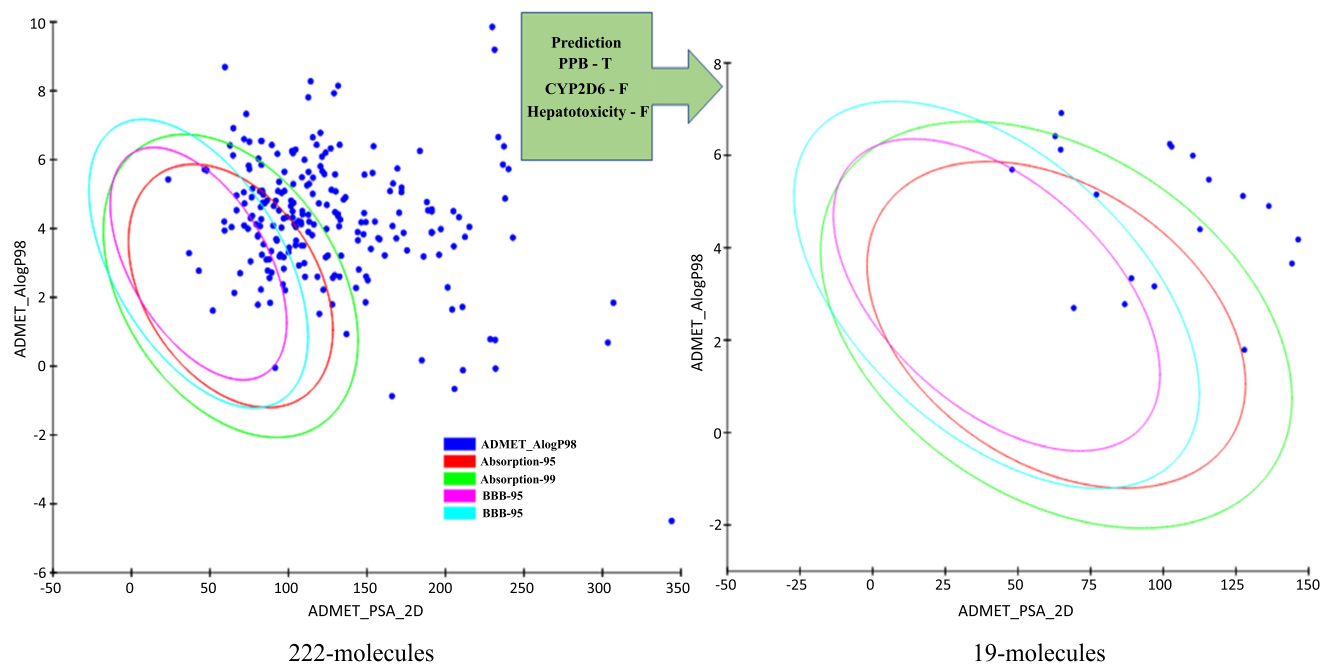


Fig. (9). 19 molecules retrieved from *in silico* pharmacokinetic properties. (*A higher resolution / colour version of this figure is available in the electronic copy of the article*).

Table 6. ADMET properties of 19 molecules.

Molecule	Solubility Level	BBB Level	Absorption Level	PPB Prediction	CYP2D6 Prediction	Hepatotoxicity Prediction
1d4s_TPV_1	1	4	2	T	F	F
1kvo_OAP_5	2	4	1	T	F	F
1vf5_TDS_2	1	4	2	T	F	F
1xdg_AB8_2	2	4	2	T	F	F
2bkt_RPF_2	3	2	0	T	F	F
2psu_MUU_1	3	4	1	T	F	F
2rew_REW_2	3	3	0	T	F	F
2x1z_PID_3	3	4	2	T	F	F
3gi4_K60_1	2	4	2	T	F	F
3gi6_D78_1	2	4	2	T	F	F
3sdi_3SD_2	3	4	2	T	F	F
3vsp_EK8_1	2	4	0	T	F	F
4d89_BXD_1	1	4	1	T	F	F
4drm_0MC_1	3	4	2	T	F	F
4dro_0MD_1	2	4	2	T	F	F
4jvf_17X_1	1	4	1	T	F	F
CDI356292	3	3	0	T	F	F
ENA752233	3	3	0	T	F	F
RG 00117	2	0	0	T	F	F

Note: F - False, and T – True

3.3.5. Molecular Docking

A CDOCKER program was used for a docking study on pdb id: 7E3H of AChE with a donepezil complex [42, 43]. The results are shown in Figs. (10A-D), displaying 2D- and 3D-interactions of donepezil at the AChE binding site, including hydrogen bond donor/acceptor and aromatic edge/face. The intense green color corresponds to the robust hydrogen bond. After the docking study, each molecule generated the ten best conformers. We further narrowed down the selection to the top 12 AChE inhibitors that exhibited a comparative advantage in terms of binding energy, as assessed by CDOCKER energy (Table 7) [44]. 3vsp_EK8_1 molecule was good with a -CDOCKER energy score of 65.6 kcal/mol, estimated activity of 223.2 nM, and fit value of 5.45. The donepezil bound with the active site residues, including Ser293, Phe295, Phe338, Tyr337, Trp86, Tyr341, Trp286, and Tyr72, with a CDOCKER energy score of 23.79 kcal/mol, and was chosen as a control. Donepezil output showed three pi-pi bonds between the aromatic residue and the benzene ring of donepezil, one hydrogen bond between hydroxyl and choline-binding pocket residue Ser293, one carbon-hydrogen bond between the carbonyl oxygen and the residue Phe295, and three pi-alkyl bonds between methyl, piperidine, and the acyl-binding pocket residues Tyr337, Phe338, and Tyr72 (Figs. 10A-D). The docking pose presented in Figs. (11A-D) of 3vsp_EK8_1 showed two hydrogen bonds between carbonyl oxygen and peripheral site residues, Phe295 and Arg296; four pi-pi bonds between benzene and choline-binding pocket residues, Trp86, Tyr341, Tyr124, and Trp286; one carbon-hydrogen bond between the carboxylic carbonyl oxygen and catalytic residue, His447, and one pi-alkyl bond between methyl and Tyr341. The 3D-interaction and 2D-interaction of 3vsp_EK8_1 at the AChE binding site, hydrogen bond donor/acceptor, and aromatic edge/face of 3vsp_EK8_1 are shown in Figs. (11A-D), respectively. 3vsp_EK8_1 showed stronger interaction with protein compared to the reference drug, *i.e.*, donepezil.

3.3.6. De Novo Evolution

The top 12 molecules generated 120 molecules as derivatives with *de novo* evolution, which were then docked back to the protein to score the -CDOCKER energy again. Table 8 displays the outcomes of the top 12 AChE inhibitors. Except for 3s-Evo_3, 1d-Evo_2, 1v-Evo_7, and 2b-Evo_3, all the molecules displayed improved energy values in comparison to the -CDOCKER energy values listed in Table 7. Fig. (12) displays the structures of the derivatives chosen after *de novo* evolution and their -CDOCKER energy score. The functional groups introduced during *de novo* evolution are enclosed in blue contour [45, 46]. After *de novo* evolution, we achieved the discovery of the most potent hit molecule 3v_evo_4, exhibiting a greater binding energy of -70.17 kcal/mol. It was observed that 3v_evo_4 interacted with crucial amino acid residues, namely Asn87, Tyr124, Trp86, Asp74, Tyr337, Tyr341, Tyr72, Ser125, His447, Arg296, Trp286, Phe295, and Val294, in addition to HOH712 and HOH715, which were found to be essential for its activity. 3v_evo_4 formed five pi-pi bonds with Tyr124, Trp86,

Tyr337, Tyr341, and Trp286, one pi-alkyl bond with Tyr72, two carbon-hydrogen bonds with His447 and Val294, four hydrogen bonds with Asn87, Ser125, Asp74, Arg296, and Phe295, and two water hydrogen bonds with HOH715 and HOH712, as shown in Figs. (13A-D). 3v_evo_4 was found to be a potential hit for AChE inhibition; hence, it may be further explored for drug development and promoted as an appropriate substitute to the present medicines employed to treat AD.

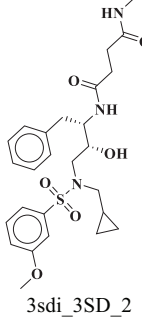
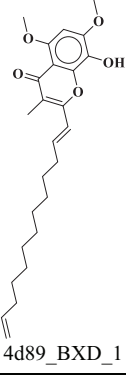
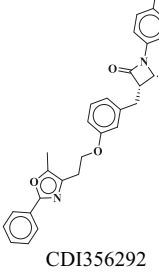
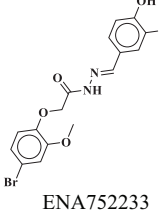
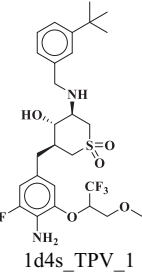
3.3.7. Molecular Simulation

CHARMM-based molecular dynamics (MD) simulations were performed by docking ligands into the active site of the AChE enzyme. We generated random ligand conformations with a 300 K temperature MD, which were later translocated into the binding site. At last, minimization was used to improve the ligand postures. With this apoprotein AChE, donepezil-AChE, 3vsp_EK8_1-AChE, and the 3v_evo_4-AChE docked complexes were subjected to MD simulation for 100 ns. The average potential energies of the apo-AChE, donepezil-AChE, 3vsp_EK8_1-AChE, and the 3v_evo_4-AChE complex were determined for equilibration and stability throughout the simulation study [47, 48]. In this study, the initial frames of apo-AChE, donepezil-AChE, 3vsp_EK8_1-AChE, and the 3v_evo_4-AChE docked complex were set as a reference, and the variability in RMSD of C_α-atoms was monitored. It was noted that the RMSD values of apo-AChE, donepezil-AChE, 3vsp_EK8_1-AChE, and the 3v_evo_4-AChE complex varied between 1.0704-6.5529, 0.67-9.6043, 0.64-6.782, and 0.6645-7.4376 Å, respectively. The average RMSD values of apo-AChE, donepezil-AChE, 3vsp_EK8_1-AChE, and the 3v_evo_4-AChE complex were 3.5001, 5.5010, 3.7955, and 3.8833 Å, respectively (Fig. 14A). The average RMSD value for donepezil was greater than that of the hit molecule, 3v_evo_4. Additionally, the average RMSD value for the screened molecule, *i.e.*, 3vsp_EK8_1, was relatively similar to that of 3v_evo_4. So, there were no substantial changes in RMSD values of unbound AChE, 3vsp_EK8_1, and 3v_evo_4 complexes. The complex of 3vsp_EK8_1, 3v_evo_4 with AChE was found to be stable. Similarly, the RMSF values of apo-AChE, donepezil-AChE, 3vsp_EK8_1-AChE, and the 3v_evo_4-AChE docked complex varied between 8.5581-15.1243, 11.2762-20.8244, 10.3362-16.8975, and 6.5203-12.5687 Å, respectively. The average RMSF values of apo-AChE, donepezil-AChE, 3vsp_EK8_1-AChE, and the 3v_evo_4-AChE complex were 10.7057, 15.7314, 14.1053, and 8.4974 Å, respectively (Fig. 14B). The average RMSF value for donepezil was higher than that of the hit molecule, 3v_evo_4. Furthermore, the average RMSD value for the screened molecule, 3vsp_EK8_1, was relatively similar to that of donepezil, but higher than that of the hit molecule. Therefore, based on the RMSF data, it was evident that the complex 3v_evo_4 exhibited greater stability compared to the other complexes. The degree of compactness, as shown by the graph of radius of gyration (Rg) with the values of apo-AChE, donepezil-AChE, 3vsp_EK8_1-AChE, and the 3v_evo_4-AChE docked complex varied between 41.3741-41.7147, 41.3894-42.9427, 41.2979-42.5917, and

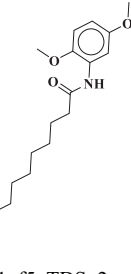
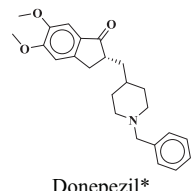
Table 7. Structure of topmost 12 molecules and reference drug (donepezil*).

Rank	Molecules	-Cdocker Energy (kcal/mol)	-Cdocker Interaction Energy (kcal/mol)	Estimated Activity (nM)	Fit Value	Interacting Amino Acids
1	 3vsp_EK8_1	65.60	77.25	223.20	5.45	Trp86, His447, Tyr341, Tyr124, Phe295, Arg296, Trp286
2	 1kvo_OAP_5	59.85	59.23	2.55	7.39	Trp86, Trp286, Tyr72, Arg296, Phe295, Val294, Tyr341, Phe338, Tyr337
3	 2psu_MUU_1	49.76	67.27	55.32	6.06	His447, Trp86, Gly121, HOH712, Asp74, Tyr124, Tyr72, Trp286
4	 RG 00117	49.69	54.77	104.15	5.78	Tyr337, Trp86, Tyr341, Phe338, Arg296, Ser293, Leu289, Trp286
5	 2rewREW_2	44.23	61.61	275.78	5.36	Trp86, Tyr133, Tyr337, His447, Phe338, HOH712, Tyr124, Phe295, Leu289, Tyr341, Trp286
6	 2bkt_RPF_2	41.77	66.60	341.20	5.27	Trp86, Glu202, Tyr337, Phe338, Tyr341, Typ286, Leu76, Ser293, Arg296, Val294

(Table 7) Contd...

Rank	Molecules	-Cdocker Energy (kcal/mol)	-Cdocker Interaction Energy (kcal/mol)	Estimated Activity (nM)	Fit Value	Interacting Amino Acids
7	 3sdi_3SD_2	39.93	69.25	906.28	4.84	Trp86, Asp74, HOH712, His447, Tyr341, Tyr337, Leu76, Trp286, Phe295
8	 4d89_BXD_1	39.57	51.49	134.13	5.67	Arg296, Phe338, Tyr337, HOH712, His447, Glu202, Trp86, Tyr124
9	 CDI356292	38.06	61.12	257.75	5.39	Tyr72, Trp286, Val294, Phe295, Trp86, His447, Phe338, Tyr341
10	 ENA752233	36.93	49.00	8.47	6.87	Leu289, Ser293, Arg296, Phe338, Tyr124, Ser125, Trp86, HOH715, Trp341, Phe295
11	 1d4s_TPV_1	35.38	55.17	703.61	4.95	Tyr337, Trp86, HOH712, Phe338, Phe296, Tyr124, Trp286, Gln291, Tyr341, Asp74, His447

(Table 7) Contd...

Rank	Molecules	-Cdocker Energy (kcal/mol)	-Cdocker Interaction Energy (kcal/mol)	Estimated Activity (nM)	Fit Value	Interacting Amino Acids
12	 1vf5_TDS_2	27.29	63.40	0.06	9.05	Trp86, His447, Tyr337, Phe338, Tyr341, Tyr72, Trp286, Val294, Ser293, Gln291, Leu289
13	 Donepezil*	23.79	58.97	*	*	Ser293, Phe295, Phe338, Tyr337, Trp86, Tyr341, Trp286, Tyr72

Note: * represents the control molecule.

all energies presented in kcal/mol.

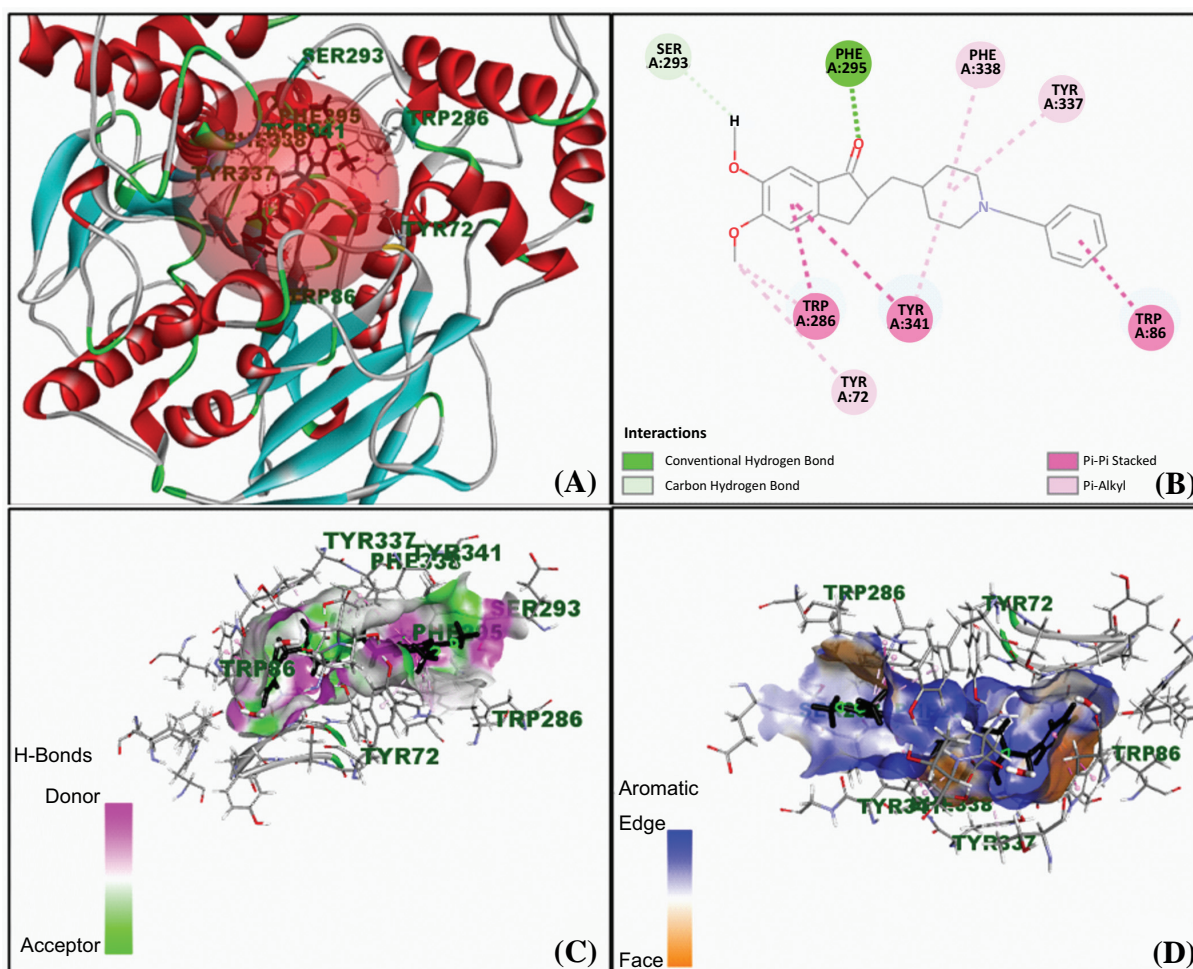


Fig. (10). (A) 3D-interaction, (B) 2D-interaction, (C) hydrogen bond donor/acceptor, and (D) aromatic edge/face of donepezil at AChE binding site. (A higher resolution / colour version of this figure is available in the electronic copy of the article).

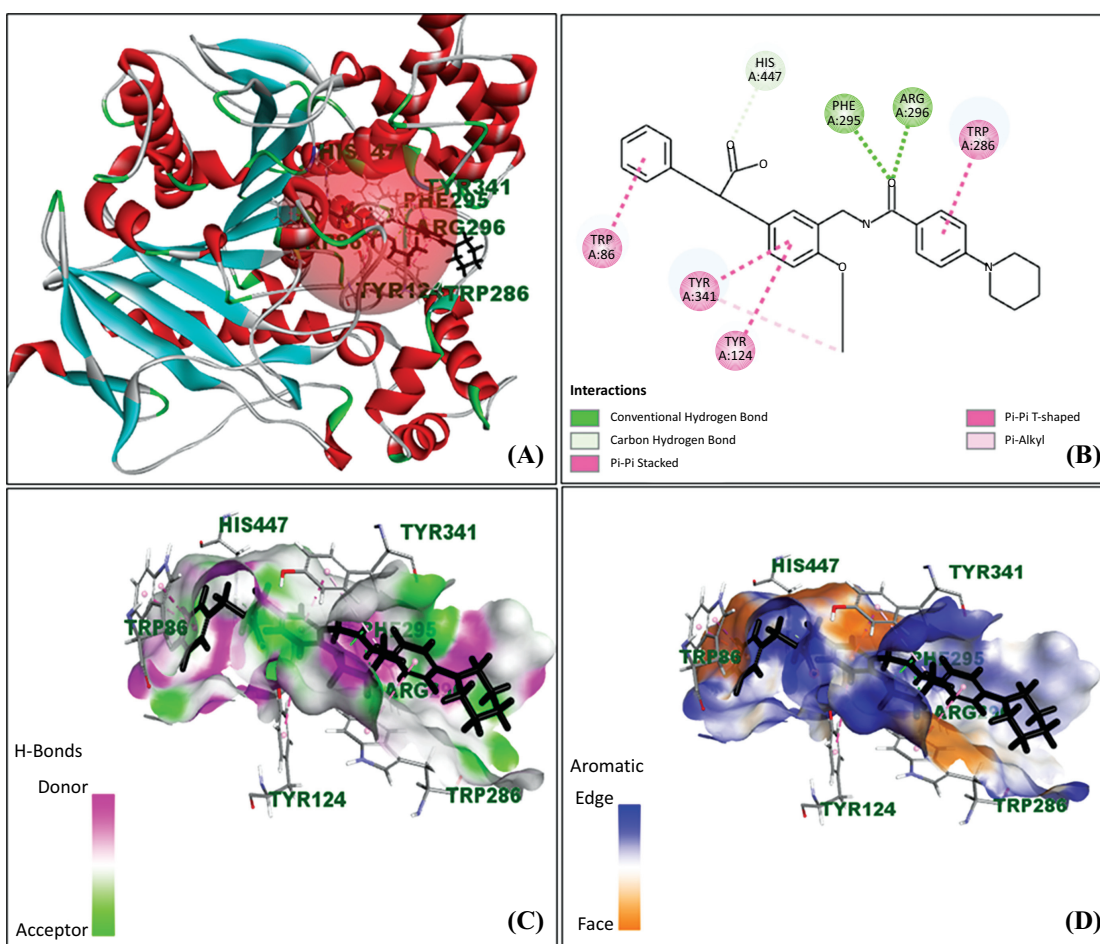


Fig. (11). (A) 3D-interaction, (B) 2D-interaction, (C) hydrogen bond donor/acceptor, and (D) aromatic edge/face of 3vsp_EK8_1 at AChE binding site. (A higher resolution / colour version of this figure is available in the electronic copy of the article).

Table 8. Molecular docking of top 12 AChE inhibitors after *de novo* evolution.

Rank	Name	-CDOCKER Energy	-CDOCKER Interaction Energy	Key Interaction Amino Acids
1	3v-Evo_4	70.17	85.16	Asn87, Tyr124, Trp86, Asp74, Tyr337, Tyr341, Tyr72, Ser125, HOH715, HOH712, His447, Arg296, Trp286, Phe295, Val294
2	1k-Evo_10	64.63	70.03	Leu76, Tyr337, Trp286, Phe295, Arg296, Tyr72, Tyr341, Phe338, Tyr124, Trp86, Asp74, Ser125, HOH715, Asn87
3	4d-Evo_10	62.15	72.05	Tyr337, His447, HOH712, Trp86, Tyr341, Asp74, Tyr72, Ser293, Tyr124, Trp286
4	C-Evo_3	54.44	68.61	Ser293, Val294, Phe295, Phe338, Tyr341, Tyr337, Tyr133, Tyr124, Trp86, Trp286, Tyr72
5	rg-Evo_8	48.80	66.86	Tyr72, Val294, Trp286, Ser293, Leu289, Tyr341, Phe338, Ser125, HOH715, Trp86, Tyr337, His447
6	2r-Evo_5	48.26	80.33	Tyr341, Trp286, HOH712, Gly121, Tyr337, His447, Phe295, Arg296, Val294
7	2p-Evo_6	48.13	80.32	His447, Trp86, Asp74, Trp286, Gln291, Tyr341, Tyr72, Leu76, Tyr124, HOH712, Gly121

(Table 8) Contd...

Rank	Name	-CDOCKER Energy	-CDOCKER Interaction Energy	Key Interaction Amino Acids
8	E-Evo_10	41.85	73.26	Leu289, Ser293, Trp286, Arg296, Phe295, Tyr124, HOH722, Trp86, His447, Gly121, Tyr341, Tyr72, Leu76
9	3s-Evo_3	26.25	76.91	Tyr337, Trp86, His447, Tyr124, Trp286, Tyr341, Val294, Pro88, HOH715, Gly121
10	1d-Evo_2	18.56	76.67	Gly121, His447, Trp86, HOH712, Phe297, Tyr337, Phe338, Leu76, Tyr341, Trp286, HOH722, Tyr124
11	1v-Evo_7	18.29	71.16	Trp86, His447, Tyr124, Tyr337, Phe338, Ser293, Gln291, Leu289, Trp286, Tyr341, Tyr72, HOH712, Gly121
12	2b-Evo_3	16.63	65.95	Gly342, Glu292, Ser293, Tyr341, Trp286, Phe338, Asp74, Tyr337, Tyr124, Tyr72, HOH712, His447, Trp86

Note: # all energies presented in Kcal/mol.

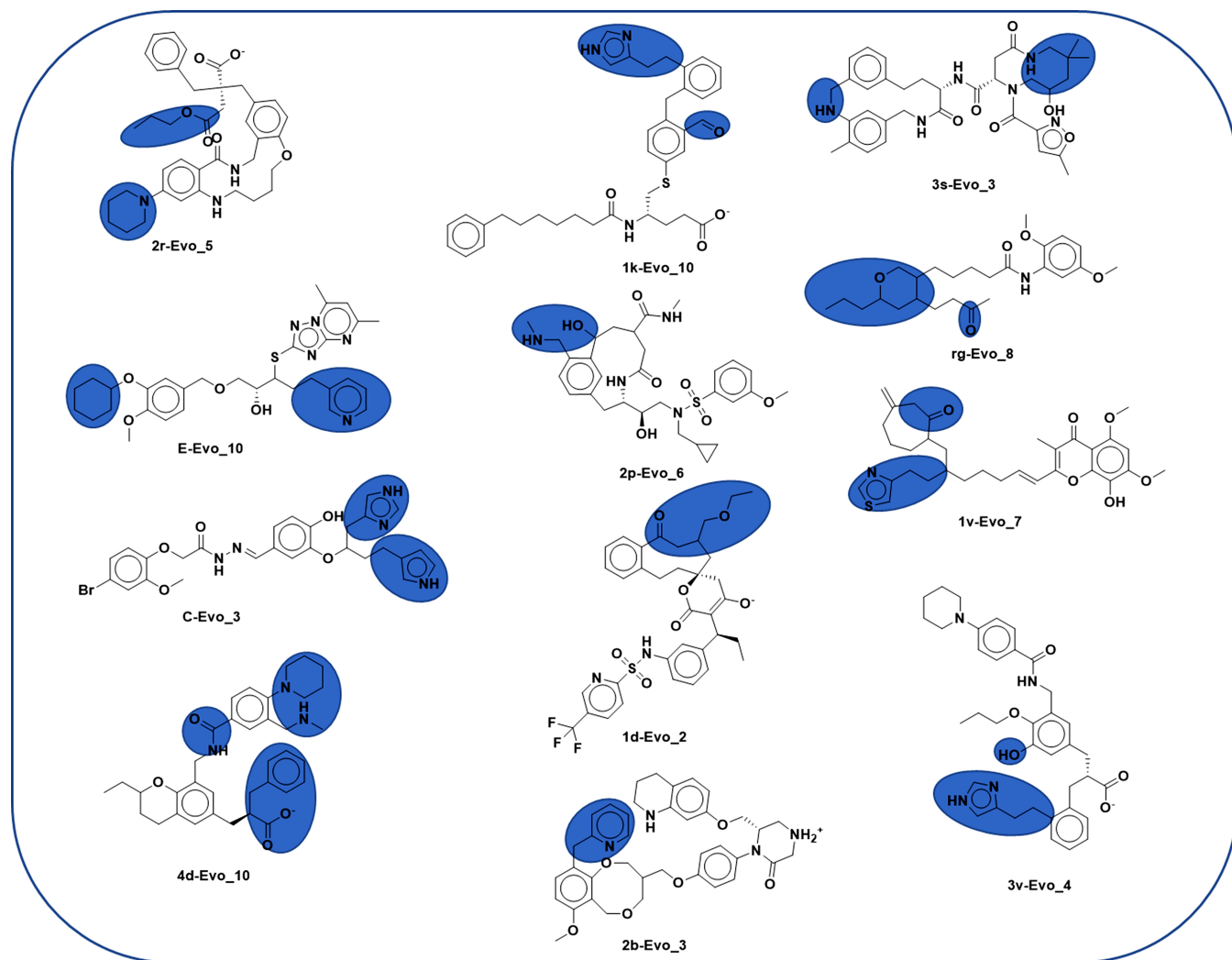


Fig. (12). Structures of 12 top molecules after *de novo* evaluation. (A higher resolution / colour version of this figure is available in the electronic copy of the article).

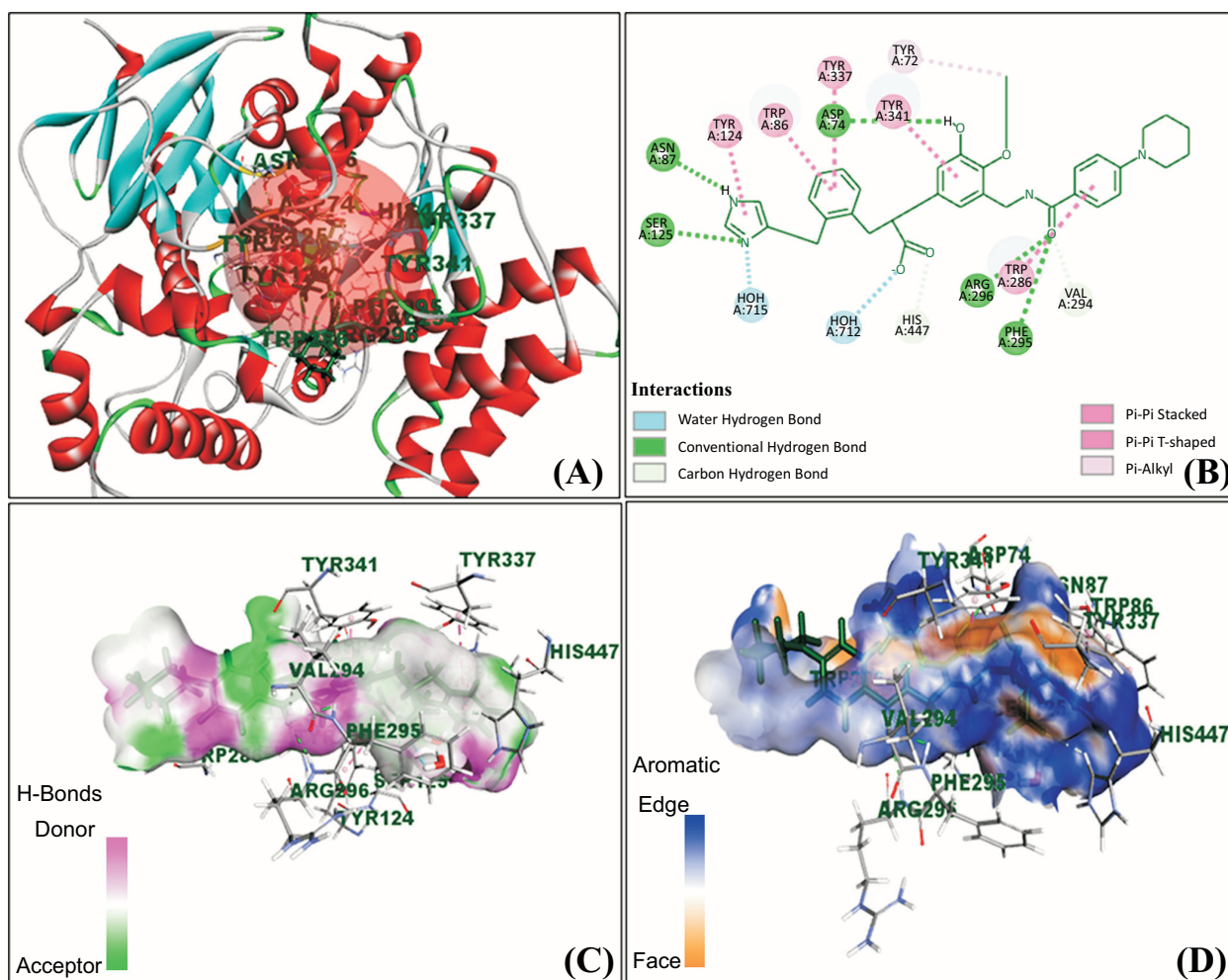


Fig. (13). (A) 3D-interaction, (B) 2D-interaction, (C) hydrogen bond donor/acceptor, and (D) aromatic edge/face of 3v-Evo_4 at AChE binding site. (A higher resolution / colour version of this figure is available in the electronic copy of the article).

41.3014–41.992 Å, respectively. The average R_g values of apo-AChE, donepezil-AChE, 3vsp_EK8_1-AChE, and the 3v_evo_4-AChE complex were 41.4979, 41.7696, 41.7623, and 41.5237 Å, respectively (Fig. 14C). Based on the R_g graph, the apoprotein (AChE enzyme) significantly overlapped with the hit molecule, *i.e.*, 3v_Evo_4. In summary, the collective results have indicated the formation of a more stable 3v_evo_4-AChE docked complex when compared to donepezil.

CONCLUSION

Alzheimer's disease is characterized by a gradual decline in cognitive abilities. The hallmark of Alzheimer's disease is AChE. Recent AChE inhibitors have gained significant attention as they are imperative in controlling central cholinergic transmission and beneficial in treating AD. We have explored AChE as a target to design its inhibitors *via* computational approaches. Using a set of 40 well-known AChE inhibitors, we have produced ten pharmacophore hypotheses. The cost analysis, Fischer's randomization, and test set have been used to verify the best pharmacophore model, *i.e.*, Hypo1, having six pharmacophore features (2 HBA, 2 HY, and 2 RA). The cost difference for Hypo1 was determined to be

58.37, and the 95% confidence range established its statistical robustness. Both the training and test sets exhibited moderately strong correlations between experimental and calculated IC_{50} values, with correlation coefficients (r^2) of 0.89 and 0.68, respectively. Additionally, the CNS Druglike, scPDB, Sample, and Minimaybridge databases were screened using Hypo1 as a 3D query. The screened molecules were initially filtered based on their estimated activity, which needed to be less than 1 nM. Subsequently, a further filtration process was carried out using ADMET analysis to select the potential molecules. Ultimately, a total of 35 molecules were selected for additional molecular docking studies. This comprehensive analysis led to a further refinement of the selection, resulting in the identification of the top 12 AChE inhibitors. These top 12 inhibitors demonstrated a comparative advantage in terms of binding energy concerning CDOCKER energy, with donepezil serving as a control for reference. Those molecules were subjected to *de novo* evolution to be re-designed with LUDI score. As a result, 3v_evo_4 modified molecule was retrieved for the 100 ns molecular simulation concerning donepezil, suggesting that the modified molecule can be recognized as the potential hit molecule for treating AD.

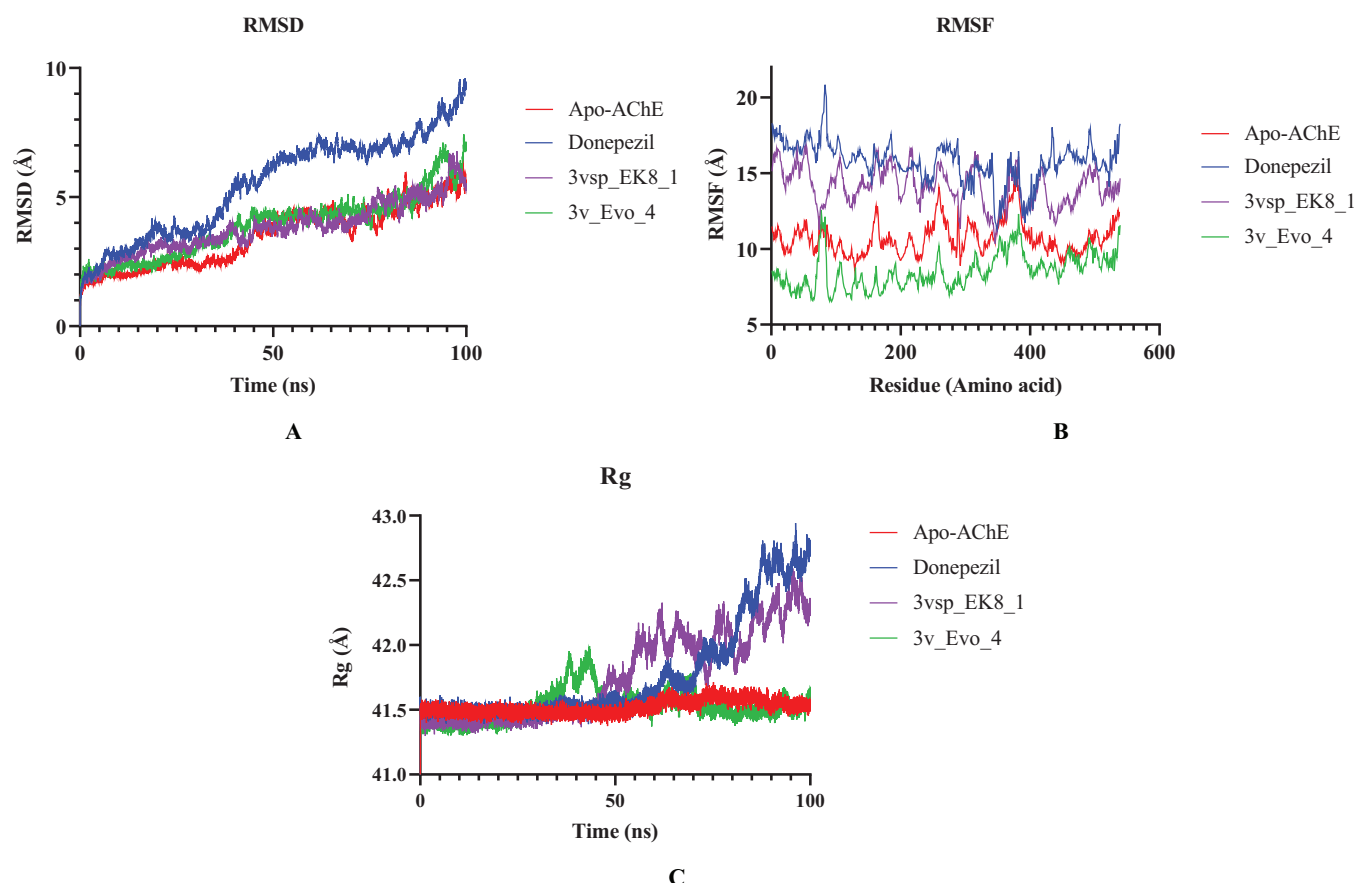


Fig. (14). Structural dynamics of molecules, including apo-AChE, donepezil, 3vsp_EK8_1, and 3v_evo_4, with the target (AChE) over 100 ns. (A) RMSD (root mean square deviation) plot. (B) RMSF (root mean square fluctuation) plot. (C) Rg (radius of gyration) plot of apo-AChE, donepezil, 3vsp_EK8_1, and 3v_evo_4, complexed with AchE, represented by a different color (red, blue, purple, and green) showing deviation concerning time (ns), fluctuation concerning amino acid residue, and degree of compactness. (A higher resolution / colour version of this figure is available in the electronic copy of the article).

AUTHORS' CONTRIBUTIONS

D.A. carried out the research work. S.K., R.A., N.B., and L.C. collected and analyzed the computational data. G.L.K. hypothesized the concept and carried out the writing of the manuscript. All the authors have read and approved the final version of the manuscript.

LIST OF ABBREVIATIONS

AD	=	Alzheimer's Disease
ACh	=	Acetylcholine
AChE	=	Acetylcholinesterase
ADMET	=	Absorption, Distribution, Metabolism, Excretion and Toxicity
CAS	=	Catalytic Active Site
CNS	=	Central Nervous System
PAS	=	Peripheral Anionic Site
HBA	=	Hydrogen Bond Acceptor
HBD	=	Hydrogen Bond Donor
HY	=	Hydrophobic
MD	=	Molecular Dynamics

RA	=	Ring Aromatic
Rg	=	Radius of Gyration
RMSD	=	Root Mean Square Deviation
RMSF	=	Root Mean Square Fluctuations

ETHICS APPROVAL AND CONSENT TO PARTICIPATE

Not applicable.

HUMAN AND ANIMAL RIGHTS

Not applicable.

CONSENT FOR PUBLICATION

Not applicable.

AVAILABILITY OF DATA AND MATERIALS

The data and supportive information are available within the article [electronic supplementary information (ESI) available for all spectroscopic data is available free of charge via the internet at <http://>].

FUNDING

None.

CONFLICT OF INTEREST

The authors declare no conflict of interest, financial or otherwise.

ACKNOWLEDGEMENTS

The authors are thankful to the Ministry of Chemical and Fertilizer, Govt. of India, for support, and to Mr. Jatin for providing valuable insights during the drafting of the article.

REFERENCES

- [1] Gong, C.X.; Dai, C.L.; Liu, F.; Iqbal, K. Multi-targets: An unconventional drug development strategy for alzheimer's disease. *Front. Aging Neurosci.*, **2022**, *14*, 837649. <http://dx.doi.org/10.3389/fnagi.2022.837649> PMID: 35222001
- [2] 2020 Alzheimer's disease facts and figures. *Alzheimers Dement.*, **2020**, *16*(3), 391-460. <http://dx.doi.org/10.1002/alz.12068>
- [3] Chen, Y.G. Research progress in the pathogenesis of alzheimer's disease. *Chin. Med. J.*, **2018**, *131*(13), 1618-1624. <http://dx.doi.org/10.4103/0366-6999.235112> PMID: 29941717
- [4] Uddin, M.S.; Kabir, M.T.; Jalouli, M.; Rahman, M.A.; Jeandet, P.; Behl, T.; Alexiou, A.; Albadrani, G.M.; Abdel-Daim, M.M.; Perveen, A.; Ashraf, G.M. Neuroinflammatory signaling in the pathogenesis of alzheimer's disease. *Curr. Neuropharmacol.*, **2022**, *20*(1), 126-146. <http://dx.doi.org/10.2174/1570159X19666210826130210> PMID: 34525932
- [5] Chaudhary, A.; Singh, V.; Varadwaj, P.K.; Mani, A. Screening natural inhibitors against upregulated G-protein coupled receptors as potential therapeutics of Alzheimer's disease. *J. Biomol. Struct. Dyn.*, **2022**, *40*(2), 673-684. <http://dx.doi.org/10.1080/07391102.2020.1817784> PMID: 32900274
- [6] Lamptey, R.N.L.; Chaulagain, B.; Trivedi, R.; Gothwal, A.; Layek, B.; Singh, J. A review of the common neurodegenerative disorders: Current therapeutic approaches and the potential role of nanotherapeutics. *Int. J. Mol. Sci.*, **2022**, *23*(3), 1851. <http://dx.doi.org/10.3390/ijms23031851> PMID: 35163773
- [7] Akbaba, E.; Bagci, E. Memory-enhancing, antioxidant, and anti-cholinesterase effects of inhaled *achillea pseudoaleppica* essential oil on scopolamine-induced amnesia rats. *J. Essent. Oil-Bear. Plants*, **2022**, *25*(4), 859-875. <http://dx.doi.org/10.1080/0972060X.2022.2121617>
- [8] Chaudhary, A.; Maurya, P.K.; Yadav, B.S.; Singh, S.; Mani, A. Current therapeutic targets for alzheimer's disease. *J. Biomed.*, **2018**, *3*, 74-84. <http://dx.doi.org/10.7150/jbm.26783>
- [9] *Global action plan on the public health response to dementia 2017 - 2025*; World Health Organization: Geneva, **2017**.
- [10] Yin, Z.; Zhang, Z.; Gao, D.; Luo, G.; Ma, T.; Wang, Y.; Lu, L.; Gao, X. Stepwise coordination-driven metal-phenolic nanoparticle as a neuroprotection enhancer for alzheimer's disease therapy. *ACS Appl. Mater. Interfaces*, **2023**, *15*(1), 524-540. <http://dx.doi.org/10.1021/acsami.2c18060> PMID: 36542560
- [11] Turgutalp, B.; Bhattacharai, P.; Ercetin, T.; Luise, C.; Reis, R.; Gurdal, E.E.; Isaak, A.; Biriken, D.; Dinter, E.; Sipahi, H.; Schepmann, D.; Junker, A.; Wünsch, B.; Sippl, W.; Gulcan, H.O.; Kizil, C.; Yarim, M. Discovery of potent cholinesterase inhibition-based multi-target-directed lead compounds for synaptoprotection in alzheimer's disease. *J. Med. Chem.*, **2022**, *65*(18), 12292-12318. <http://dx.doi.org/10.1021/acs.jmedchem.2c01003> PMID: 36084304
- [12] Rao, YL; Ganaraja, B; Murlimanju, B V; Joy, T; Krishnamurthy, A; Agrawal, A Hippocampus and its involvement in Alzheimer's disease: A review. *3 Biotech*, **2022**, *12*(2), 55.
- [13] Serrano-Pozo, A.; Frosch, M.P.; Masliah, E.; Hyman, B.T. Neuro-pathological alterations in Alzheimer disease. *Cold Spring Harb. Perspect. Med.*, **2011**, *1*(1), a006189. <http://dx.doi.org/10.1101/cshperspect.a006189> PMID: 22229116
- [14] Rossi, M.; Freschi, M.; de Camarga, N.L.; Salerno, A.; de Melo Viana, T.S.; Nachon, F.; Chantegrel, F.; Soukup, O.; Prchal, L.; Malaguti, M.; Bergamini, C.; Bartolini, M.; Angeloni, C.; Hrelia, S.; Soares Romeiro, L.A.; Bolognesi, M.L. Sustainable drug discovery of multi-target-directed ligands for alzheimer's disease. *J. Med. Chem.*, **2021**, *64*(8), 4972-4990. <http://dx.doi.org/10.1021/acs.jmedchem.1c00048> PMID: 33829779
- [15] Tran, K.N.; Nguyen, N.P.K.; Nguyen, L.T.H.; Shin, H.M.; Yang, I.J. Screening for neuroprotective and rapid antidepressant-like effects of 20 essential oils. *Biomedicines*, **2023**, *11*(5), 1248. <http://dx.doi.org/10.3390/biomedicines11051248> PMID: 37238920
- [16] Miles, J.A.; Ross, B.P. Recent advances in virtual screening for cholinesterase inhibitors. *ACS Chem. Neurosci.*, **2021**, *12*(1), 30-41. <http://dx.doi.org/10.1021/acschemneuro.0c00627> PMID: 33350300
- [17] Costanzi, S.; Machado, J.H.; Mitchell, M. Nerve agents: What they are, how they work, how to counter them. *ACS Chem. Neurosci.*, **2018**, *9*(5), 873-885. <http://dx.doi.org/10.1021/acschemneuro.8b00148> PMID: 29664277
- [18] Oset-Gasque, M.J.; Marco-Contelles, J. Alzheimer's disease, the "one-molecule, one-target" paradigm, and the multitarget directed ligand approach. *ACS Chem. Neurosci.*, **2018**, *9*(3), 401-403. <http://dx.doi.org/10.1021/acschemneuro.8b00069> PMID: 29465220
- [19] Kwong, H.C.; Chidan Kumar, C.S.; Mah, S.H.; Mah, Y.L.; Chia, T.S.; Quah, C.K.; Lim, G.K.; Chandraju, S. Crystal correlation of heterocyclic imidazo[1,2-a]pyridine analogues and their anticholinesterase potential evaluation. *Sci. Rep.*, **2019**, *9*(1), 926. <http://dx.doi.org/10.1038/s41598-018-37486-7> PMID: 30700752
- [20] Khan, M.T.H. Molecular interactions of cholinesterases inhibitors using *in silico* methods: Current status and future prospects. *N. Biotechnol.*, **2009**, *25*(5), 331-346. <http://dx.doi.org/10.1016/j.nbt.2009.03.008> PMID: 14941049
- [21] Mariki, A.; Anaeigoudari, A.; Zahedifar, M.; Pouramiri, B.; Ayati, A.; Lotfi, S. Design, green synthesis, and biological evaluation of new substituted tetrahydropyrimidine derivatives as acetylcholinesterase inhibitors. *Polycycl. Aromat. Compd.*, **2022**, *42*(8), 5231-5241. <http://dx.doi.org/10.1080/10406638.2021.1933102>
- [22] Ahmad, S.; Iftikhar, F.; Ullah, F.; Sadiq, A.; Rashid, U. Rational design and synthesis of dihydropyrimidine based dual binding site acetylcholinesterase inhibitors. *Bioorg. Chem.*, **2016**, *69*, 91-101. <http://dx.doi.org/10.1016/j.bioorg.2016.10.002> PMID: 27750058
- [23] Akincioğlu, H.; Gülcin, İ. Potent acetylcholinesterase inhibitors: Potential drugs for alzheimer's disease. *Mini Rev. Med. Chem.*, **2020**, *20*(8), 703-715. <http://dx.doi.org/10.2174/1389557520666200103100521> PMID: 31902355
- [24] BIOVIA. *Dassault Systèmes*; BIOVIA Discovery Studio: San Diego, **2022**.
- [25] Li, Z.; Wan, H.; Shi, Y.; Ouyang, P. Personal experience with four kinds of chemical structure drawing software: review on ChemDraw, ChemWindow, ISIS/Draw, and ChemSketch. *J. Chem. Inf. Comput. Sci.*, **2004**, *44*(5), 1886-1890. <http://dx.doi.org/10.1021/ci049794h> PMID: 15446849
- [26] Gao, H.; Jiang, Y.; Zhan, J.; Sun, Y. Pharmacophore-based drug design of AChE and BChE dual inhibitors as potential anti-Alzheimer's disease agents. *Bioorg. Chem.*, **2021**, *114*(March), 105149. <http://dx.doi.org/10.1016/j.bioorg.2021.105149> PMID: 34252860
- [27] Opo, F.A.D.M.; Rahman, M.M.; Ahammad, F.; Ahmed, I.; Bhuiyan, M.A.; Asiri, A.M. Structure based pharmacophore modeling, virtual screening, molecular docking and ADMET approaches for identification of natural anti-cancer agents targeting XIAP protein. *Sci. Rep.*, **2021**, *11*(1), 1-18. <http://dx.doi.org/10.1016/j.bioorg.2021.105149> PMID: 33414495
- [28] Hosseini, F.; Mohammadi-Khanapostani, M.; Azizian, H.; Ramaniz, A.; Tehrani, M.B.; Nadri, H.; Larijani, B.; Biglar, M.; Adibi, H.; Mahdavi, M. 4-Oxobenzo[d]1,2,3-triazin-pyridinium-phenylacetamide derivatives as new anti-Alzheimer agents: Design,

- synthesis, *in vitro* evaluation, molecular modeling, and molecular dynamic study. *Struct. Chem.*, **2020**, 31(3), 999-1012.
<http://dx.doi.org/10.1007/s11224-019-01472-0>
- [29] Dileep, K.V.; Chiemi, K.I.; Mutsuko, M-T.; Mayumi, K-N.; Yonemochi, K.; Hanada, M.S. Discovery, Crystal structure of human acetylcholinesterase in complex with tacrine. Implic drug Macromol. *Int. J. Biol.*, **2022**, 210, 172-181.
 PMID: 35526766
- [30] Wu, G.; Robertson, D.H.; Brooks, C.L., III; Vieth, M. Detailed analysis of grid-based molecular docking: A case study of CDOCKER—A CHARMM-based MD docking algorithm. *J. Comput. Chem.*, **2003**, 24(13), 1549-1562.
<http://dx.doi.org/10.1002/jcc.10306> PMID: 12925999
- [31] Gupta, A.; Müller, A.T.; Huisman, B.J.H.; Fuchs, J.A.; Schneider, P.; Schneider, G. Generative recurrent networks for *de novo* drug design. *Mol. Inform.*, **2018**, 37(1-2), 1700111.
<http://dx.doi.org/10.1002/minf.201700111> PMID: 29095571
- [32] Böhm, H.J. LUDI: Rule-based automatic design of new substituents for enzyme inhibitor leads. *J. Comput. Aided Mol. Des.*, **1992**, 6(6), 593-606.
<http://dx.doi.org/10.1007/BF00126217> PMID: 1291628
- [33] Muegge, I. PMF scoring revisited. *J. Med. Chem.*, **2006**, 49(20), 5895-5902.
<http://dx.doi.org/10.1021/jm050038s> PMID: 17004705
- [34] Brown, T. Design thinking. *Harv. Bus. Rev.*, **2008**, 86(6), 84-92, 141.
 PMID: 18605031
- [35] Krammer, A.; Kirchhoff, P.D.; Jiang, X.; Venkatachalam, C.M.; Waldman, M. LigScore: A novel scoring function for predicting binding affinities. *J. Mol. Graph. Model.*, **2005**, 23(5), 395-407.
<http://dx.doi.org/10.1016/j.jmgm.2004.11.007> PMID: 15781182
- [36] Phillips, J.C.; Braun, R.; Wang, W.; Gumbart, J.; Tajkhorshid, E.; Villa, E.; Chipot, C.; Skeel, R.D.; Kalé, L.; Schulten, K. Scalable molecular dynamics with NAMD. *J. Comput. Chem.*, **2005**, 26(16), 1781-1802.
<http://dx.doi.org/10.1002/jcc.20289> PMID: 16222654
- [37] BindingDB. Available from: <https://www.bindingdb.org/rwd/bind/index.jsp>
- [38] Schuler, J.; Hudson, M.; Schwartz, D.; Samudrala, R. A systematic review of computational drug discovery, development, and repurposing for ebola virus disease treatment. *Molecules*, **2017**, 22(10), 1777.
<http://dx.doi.org/10.3390/molecules22101777> PMID: 29053626
- [39] Hussein, R.K.; Elkhair, H.M. Molecular docking identification for the efficacy of some zinc complexes with chloroquine and hydroxychloroquine against main protease of COVID-19. *J. Mol. Struct.*, **2021**, 1231, 129979.
- [40] Yan, G.; Li, D.; Zhong, X.; Liu, G.; Wang, X.; Lu, Y.; Qin, F.; Guo, Y.; Duan, S.; Li, D. Identification of HDAC6 selective inhibitors: Pharmacophore based virtual screening, molecular docking and molecular dynamics simulation. *J. Biomol. Struct. Dyn.*, **2021**, 39(6), 1928-1939.
<http://dx.doi.org/10.1016/j.molstruc.2021.129979> PMID: 33518801
- [41] Kalita, J.; Chetia, D.; Rudrapal, M. Molecular docking, drug-likeness studies and ADMET prediction of quinoline imines for antimalarial activity. *J. Med. Chem. Drug Des.*, **2019**, 2(1), 1-7.
 Fernandes, P.A.; Passos, Ó.; Ramos, M.J. Necessity is the mother of invention: A remote molecular bioinformatics practical course in the COVID-19 era. *J. Chem. Educ.*, **2022**, 99(5), 2147-2153.
<http://dx.doi.org/10.1021/acs.jchemed.1c01195> PMID: 35529516
- [42] Hartshorn, M.J.; Verdonk, M.L.; Chessari, G.; Brewerton, S.C.; Mooij, W.T.M.; Mortenson, P.N.; Murray, C.W. Diverse, high-quality test set for the validation of protein-ligand docking performance. *J. Med. Chem.*, **2007**, 50(4), 726-741.
<http://dx.doi.org/10.1021/jm061277y> PMID: 17300160
- [43] Al-Khafaji, K.; Taskin Tok, T. Amygdalin as multi-target anti-cancer drug against targets of cell division cycle: Double docking and molecular dynamics simulation. *J. Biomol. Struct. Dyn.*, **2021**, 39(6), 1965-1974.
<http://dx.doi.org/10.1080/07391102.2020.1742792> PMID: 32174270
- [44] Böhm, H-J. The computer program LUDI: A new method for the *de novo* design of enzyme inhibitors. *J. Comput. Aided Mol. Des.*, **1992**, 6(1), 61-78.
<http://dx.doi.org/10.1007/BF00124387> PMID: 1583540
- [45] Muegge, I.; Martin, Y.C. A general and fast scoring function for protein-ligand interactions: A simplified potential approach. *J. Med. Chem.*, **1999**, 42(5), 791-804.
<http://dx.doi.org/10.1021/jm980536j> PMID: 10072678
- [46] Jabir, N.R.; Rehman, M.T.; Alsolami, K.; Shakil, S.; Zugaibi, T.A.; Alserihi, R.F.; Khan, M.S.; AlAjmi, M.F.; Tabrez, S. Concatenation of molecular docking and molecular simulation of BACE-1, γ -secretase targeted ligands: In pursuit of Alzheimer's treatment. *Ann. Med.*, **2021**, 53(1), 2332-2344.
<http://dx.doi.org/10.1080/07853890.2021.2009124> PMID: 34889159
- [47] Shahwan, M.; Khan, M.S.; Husain, F.M.; Shamsi, A. Understanding binding between donepezil and human ferritin: Molecular docking and molecular dynamics simulation approach. *J. Biomol. Struct. Dyn.*, **2022**, 40(9), 3871-3879.
<http://dx.doi.org/10.1080/07391102.2020.1851302> PMID: 33228460